CHALMERS
UNIVERSITY OF TECHNOLOGY

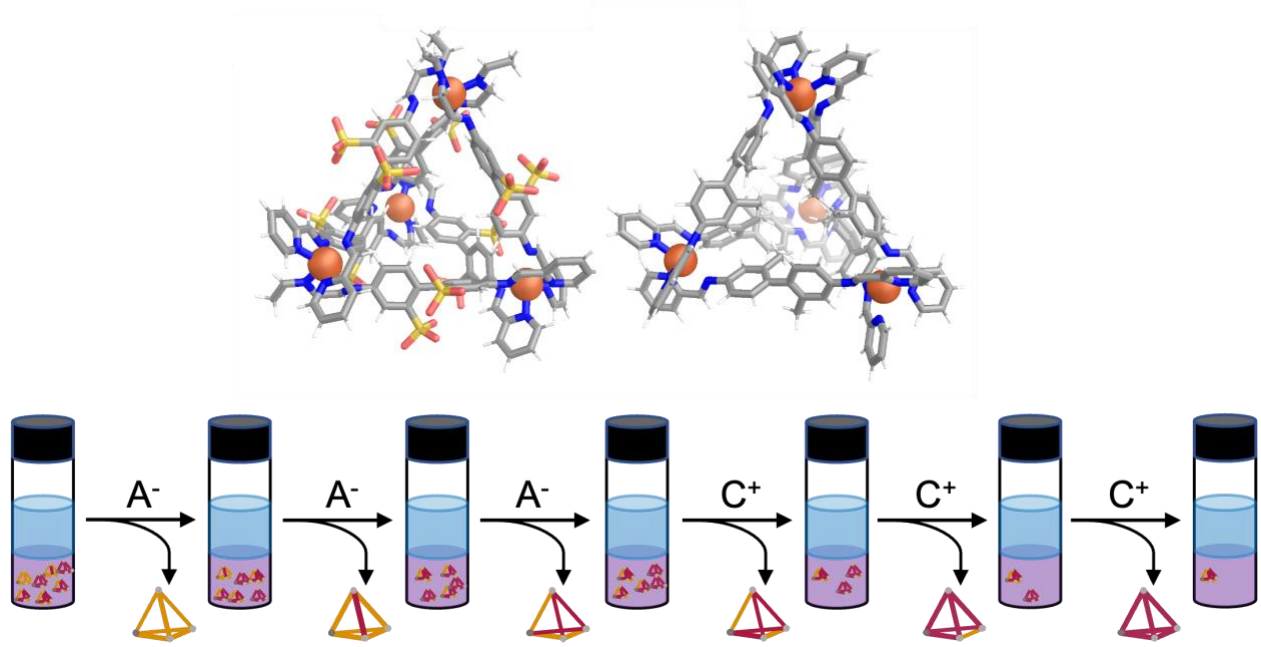

Towards a novel route for preparing heteroleptic coordination cages

Phase transfer of anionic and heteroleptic M_4L_6 tetrahedra

Master's thesis in Materials Chemistry

Ebba Matic

DEPARTMENT OF CHEMISTRY AND CHEMICAL ENGINEERING
Division of chemistry and biochemistry

CHALMERS UNIVERSITY OF TECHNOLOGY
Gothenburg, Sweden 2023
www.chalmers.se

Towards a novel route for preparing heteroleptic coordination cages
Phase transfer of anionic and heteroleptic M_4L_6 tetrahedra

EBBA MATIC

Department of Chemistry and Chemical Engineering

Division of Chemistry and Biochemistry

CHALMERS UNIVERSITY of TECHNOLOGY

Gothenburg, Sweden 2023

Towards a new route for preparing heteroleptic coordination cages
Phase transfer of anionic and heteroleptic M_4L_6 tetrahedra

Supervisor: Angela Grommet, Division of Chemistry and Biochemistry, Chalmers University of Technology,

Examiner: Gunnar Westman, Division of Chemistry and Biochemistry, Chalmers University of Technology

Master's Thesis 2023
Department of Chemistry and Chemical engineering

Chalmers University of Technology

SE-412 96 Gothenburg

Telephone +46 31 772 1000

Cover: Crystal structures of the two cages studied in this work, and separation of a heteroleptic library with phase transfer

Towards a novel route for preparing heteroleptic coordination cages
Phase transfer of anionic and heteroleptic M_4L_6 tetrahedra

Ebba Matic

Department of Chemistry and Chemical Engineering Chalmers University of Technology

Abstract

Heteroleptic coordination cages, discrete assemblies of different organic ligands (L) and metal centers (M), are one of the most promising types of structures for use as synthetic enzymes. The central cavity of a heteroleptic coordination cage has a lower symmetry than that of conventional coordination cages, and the structure can be designed for specific applications by variation of the ligands. One problem with using heteroleptic coordination cages, however, is the significant synthetic effort required to rationally design and assemble the cage, and make sure that only the desired product forms. If heteroleptic cages could instead be synthesized as a library of different species, and then separated, heteroleptic coordination cages could be used more widely.

This project takes the first steps towards a novel route for preparing heteroleptic coordination cages from a coordination cage library, separated by counter ion driven phase transfer. As a proof of principle $Fe_4L_{(6-n)}L'_n$ tetrahedra, formed through subcomponent self-assembly from two geometrically similar amine components and one aldehyde component, were prepared (making ligands L and L'). First the homoleptic cages Fe_4L_6 and $Fe_4L'_6$ were prepared, subsequently a heteroleptic library was prepared by combining the two ligands. The resulting library contains homo- and heteroleptic cage species with different charges and cavity sizes. These cages were then transferred from a water solution to an immiscible organic solvent by counterion induced phase transfer.

The phase transfer was followed with UV-Vis spectroscopy and slice selective nuclear magnetic resonance (NMR) spectroscopy. The homoleptic anionic $Fe_4L_6^{4-}$ cage was found to be too hydrophilic to phase transfer. The aldehyde component was therefore replaced with a more hydrophobic, methylated aldehyde. This cage could be transferred to ethyl acetate (EtOAc) with the quaternary amine salts cetrimonium bromide (CTAB) and didodecyldimethylammonium bromide (DDAB). The homoleptic cationic $Fe_4L'_6^{8+}$ cage was transferred from water to EtOAc using lithium tetrakis(pentafluorophenyl)borate ethyl etherate ($LiB(C_6F_5)_4$), as in previous studies. When $LiB(C_6F_5)_4$ was added to a two-phase system containing the cage library in water and ethyl acetate, some cage species were transferred. The identities of these could not be determined due to the low concentrations. In future studies the transferred heteroleptic species could be characterized by NMR, mass spectrometry and X-ray diffraction. The impact of the salt on phase transfer, and communication between cages of opposite charges will also be investigated.

Keywords: heteroleptic coordination cages, phase transfer,

Acknowledgements

First, I would like to thank my supervisor, Angela Grommet. Thank you for pushing me when I need it and reining me in when my thoughts are spinning. And thank you for being as excited as I am about my interesting results. I am so excited to continue to work, learn from and grow with you for the next five years!

Thank you to Lars Öhrström for the help with the X-ray diffraction measurements and solving the crystal structure.

To the rest of the Grommet group, thank you for sharing the joys and hardships of working with coordination cages with me! I'm so proud of what we have achieved in these short months. Bachelor's collective, thank you for reminding me to be excited about my work, even about the small things.

Lastly, thank you to my family and friends for putting up with me when all I can think about is coordination cages and for supporting me throughout the project.

Ebba Matic, Gothenburg, May 2023

Abbreviations

ButOH	1-butanol
CTAB	Cetrimonium bromide
D_2O	Deuturated water
DDAB	Didodecyldimethylammonium bromide
EtOAc	Ethyl acetate
$Li[B(C_6F_5)_4]$	Lithium tetrakis(pentafluorophenyl)borate ethyl etherate
Me	Methyl group
NMR	Nuclear magnetic resonance
$P(C_6H_{13})_3(C_{14}H_{29})Cl$	Trihexyltetradecylphosphonium chloride
$P(C_6H_5)_4Cl$	Tetraphenylphosphonium chloride
SO_3^-	Sulfonate group

Table of Contents

1 Introduction

In nature, proteins perform many different functions, such as molecular recognition as receptors and catalysis as enzymes. In nature, these functions are highly specific and efficient as the proteins have evolved to fit the substrate perfectly. Scientists now want to design artificial systems that mimic the selectivity and efficiency of enzymes for use in catalysis, but this is very difficult to achieve. One class of molecules that has gained attention for use as artificial enzymes are coordination cages, a class of supramolecular assemblies with metal centers connected by organic ligands, arranged in discrete polyhedra [1]. Inside the cage there is a cavity that can be tailored for use in many different applications. For example, a cage can be designed to (selectively) encapsulate a guest for stabilization [2] or separation [3], or be used for shape- and size-selective catalysis [4, 5]. One problem, however, is that the cavity of a coordination cage has a very high symmetry while efficiency of enzymes comes from the very low symmetry of the binding sites. A lower symmetry of the cavity can be achieved by having two or more types of ligands in the cage, this is called a heteroleptic coordination cage [6].

Cage formation is a self-assembly process where reversible metal-ligand bonds form [1]. Due to the reversible nature of the bonds that form in the self-assembly reaction, there is a built-in error checking in the process. If a bond that does not belong to the most favorable product forms, it will break and the final product can either be the most kinetically or the most thermodynamically stable structure(s), depending on the system. Subcomponent self-assembly is a type of cage formation where the ligand is formed in situ, via templating on the metal center. In these reactions, in addition to metal-ligand bonds, dynamic covalent bonds in the ligands are formed [7]. There are three possible outcomes from the cage self-assembly. The first one is that only the most stable product forms. The second is that a mixture of cages with different structures or compositions form, where all products are stable. The distribution of the species will reflect the statistical distribution of the structures based on their relative energies. The last possibility is that a mixture of different, interconverting, species at equilibrium forms.

The shape of the coordination cage is affected by many factors. The two most important are the ligand structure and the coordination geometry of the metal centers (e.g. square planar for Pd(II) and octahedral for Fe(II)) [1]. Other factors that can influence the cage structure are the counter ions, the solvent used and if there are guest molecules present. The many factors influencing the cage structure make rational design of coordination cages difficult. Carefully designed, often rigid, ligands are combined with metal centers with a predictable geometry. This strategy generally requires a large synthetic effort and limits the types of ligands that can be used. Design of heteroleptic cages is especially challenging. To rationally design them, the ligands and metal centers should fit together like puzzle pieces, so that the only product is the desired one.

Previously Grommet et al. [8] have shown that cationic coordination cages can be transferred from aqueous phase to an organic phase using anion exchange. When (tetrakis(pentafluoro-phenyl) borate ($B(C_6F_5)_4^-$) was added to a two-phase system containing ethyl acetate (EtOAc) and a water solution of a cage, the cage coordinated with $B(C_6F_5)_4^-$, became hydrophobic and was redistributed to the ethyl acetate phase. By subsequent addition of a hydrophilic anion, e.g., sulfate, the cage could be transferred back to the water phase. This phase transfer method can be used for otherwise difficult separations, by encapsulating a guest and then transporting it to another phase.

In this work I am interested in extending the work of Grommet et al. to anionic cages, and to separate heteroleptic cages. This method will be used as a step in a novel route for preparing of heteroleptic

cages. A statistical mixture of heteroleptic cages is obtained by mixing different ligands with metal ions in the cage assembly reaction. The desired cage is then separated out using stimuli induced phase transfer. This method would make low symmetry coordination cages accessible without the need for large synthetic efforts.

1.1 Purpose and aims

In this project I aim to extend the work of Grommet et. al [8] to anionic cages and mixtures of heteroleptic cages, with the goal of developing a new route for preparation of heteroleptic coordination cages. As a proof of principle, homoleptic cages **4** and **5** (Figure 1) (formed from aldehyde **1** and diamines **2** and **3**, respectively) and a library of heteroleptic coordination cages (Figure 2) with the same ligands will be studied. The heteroleptic cage library formed by combining these two ligands with the same overall geometry will contain species with a range of different charges. In addition to a range of charges, this library will also contain species with a range of cavity sizes. There is some conformational freedom in the bonds of the ligand, and the orientation of the substituents can change to optimize the interactions with the surrounding water. The SO_3^- groups of cage **4** will be oriented away from the cavity, while the Me-groups of cage **5** will prefer to be oriented towards the hydrophobic internal cavity.

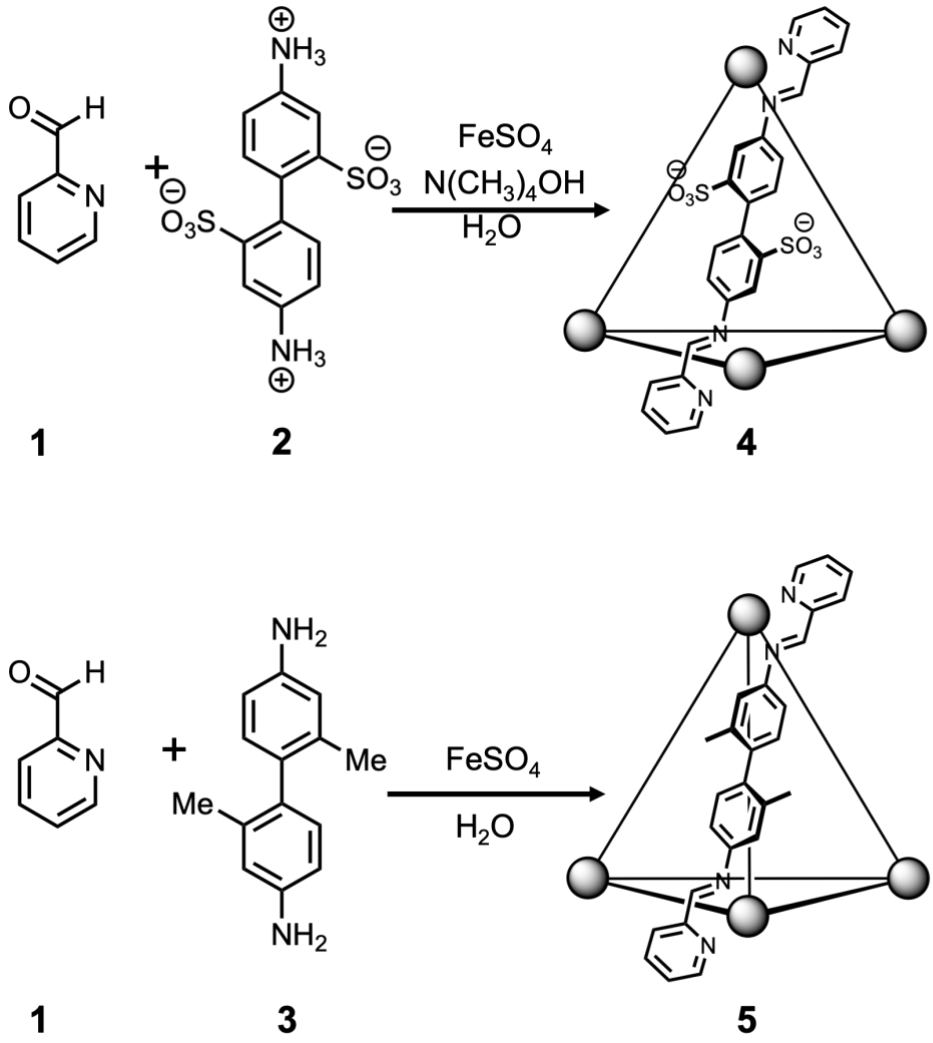

Figure 1. Synthesis of two homoleptic cage species from aldehyde 1 and amines 2 or 3, respectively

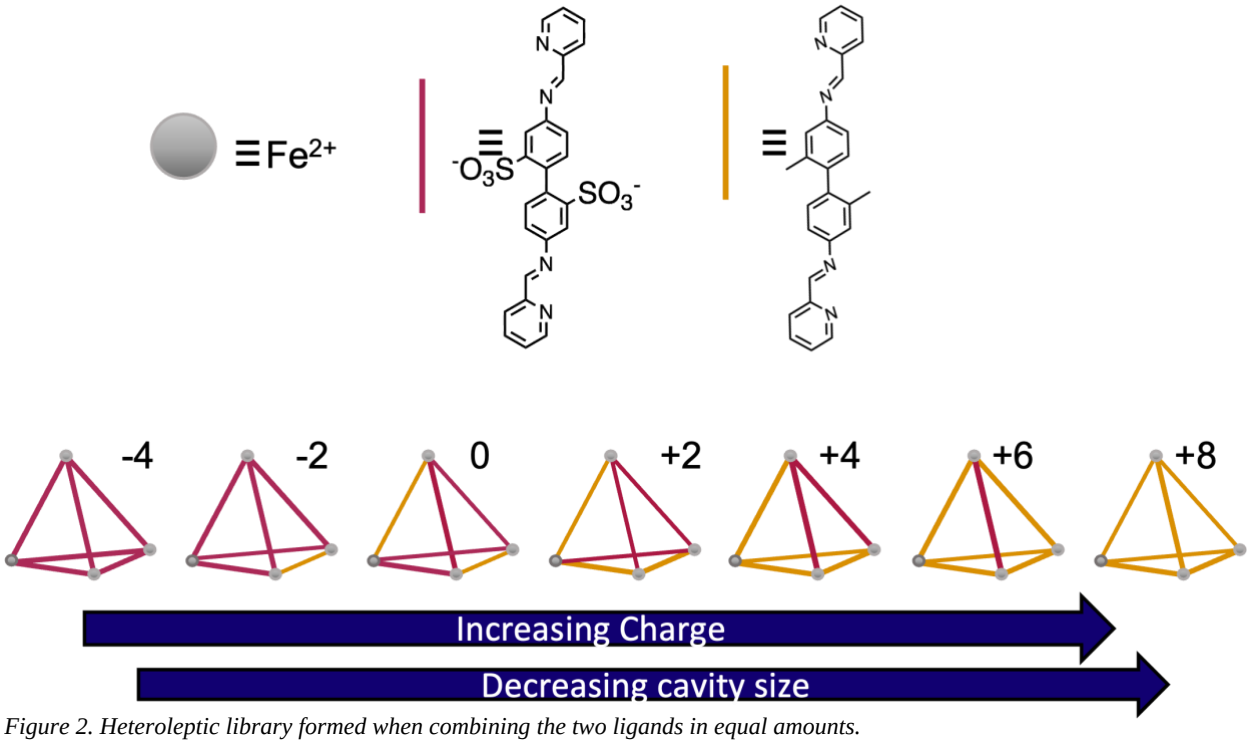

Figure 2. Heteroleptic library formed when combining the two ligands in equal amounts.

The phase transfer method developed by Grommet et al. [8] can be used to separate mixtures of cage. In mixtures of cages different species transfer sequentially based on charge (higher charge first) and charge density. As there are species with a range of charges, they can be sequentially transported from a water phase to an organic phase and subsequently isolated (Figure 3). This system is a good proof of principle as there are commercially available subcomponents with the same geometry but with different charges. Additionally, cage **4** is known to be stable in a water solution [7]. Additionally, this cage is made up of low spin iron, making characterization with NMR easier [1]. Due to the presence of low spin iron-imine coordination the cage complexes will have a dark purple color. This means that phase transfer of the cages can be monitored visually, or by means of UV-Vis absorption.

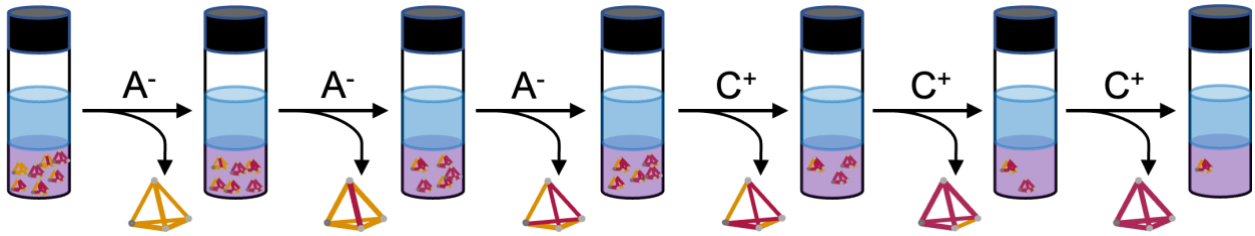

Figure 3. Schematic representation of anion driven phase transfer in a two-phase system for separation of heteroleptic coordination cages.

2 Background

This chapter provides a background on supramolecular chemistry, with a focus on coordination cages. The structure, design, solution behavior and characterization of different coordination cages will also be introduced.

2.1 Supramolecular Chemistry

Supramolecular chemistry is often described as "chemistry beyond the molecule" [9]. Unlike in conventional chemistry, where the focus is on molecules build up from covalent bond between molecules, in supramolecular chemistry, interactions between molecules, such as hydrogen bonds, electrostatic interactions and van der Waals interactions, are used to build new entities with properties different, and often better, than those of the components [10]. The weak interactions holding supramolecular assemblies together give rise to a range of interesting properties. For example, many supramolecular systems are self-healing and stimuli responsive due to the weak bonds holding the supramolecules together [10]. Supramolecular chemistry has found applications in sensing, catalysis, and separations [11].

The basis of the first supramolecular chemistry was a lock and key principle, where a guest molecule fits in a host molecule like a key in a lock (Figure 4 a) [10]. This is how enzymes are proposed to work. This principle was first proposed by Emil Fischer in 1894. In the 1960s this was extended to artificial molecules; Charles Pedersen observed that a crown ether showed molecular recognition. Donald Cram extended this recognition to a wide range of systems, and this was the beginning of host-guest chemistry. In 1978 the French chemist Jean-Marie Lehn coined the term supramolecular chemistry to cover the novel chemistries based on molecular recognition. Pedersen, Cram and Lehn where awarded the Nobel prize in chemistry for their contributions in the field. Today there are many different types of supramolecular systems, with varied shapes, sizes, and functions. Examples of supramolecules made up of only a few molecules include rotaxanes, cyclic molecules threaded on a linear molecule, and catenane, a supramolecule made up of entangled rings, and coordination cages, discrete structures made up of metal centres bridged by ligands. The functions of these systems are based on shape control. Examples of larger supramolecules are metal-organic frameworks (MOFs), vesicles, micelles and membranes. It is common for supramolecules, especially large ones, to form in self-assembly reactions [10]. A self-assembly reaction is a spontaneous formation of a structure when the components are combined. The final product is controlled by the thermodynamics of the system and the kinetics of the formation.

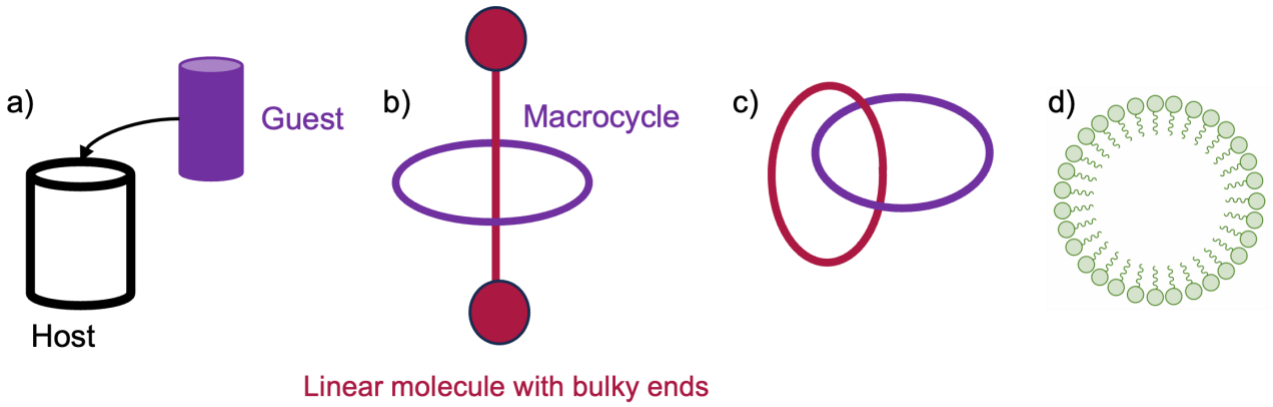

Figure 4. Schematic representations of some supramolecules. a) Host guest system. b) Rotaxane, a linear molecule threaded through a macrocycle c) Catenane, two entangled macrocycles. d) Micelle, a spherical assembly of amphiphilic molecules.

2.2 Coordination Cages

A coordination cage consists of metal ions (M) linked by organic ligands (L), assembled into a discrete structure [1]. The ligands can bridge the metal centres either along an edge of the structure or across the face. The first coordination cage was reported by Saalfrank et al. in 1988 [12]. They obtained this cage as an intermediate when trying to synthesize allenes, in a reaction between diethyl malonate with oxalyl chloride in the presence of methylmagnesium iodide as a base. This intermediate, **6,** had a surprisingly high symmetry and was the first cage compound (Figure 5). Since the discovery of the first tetrahedral coordination cage, numerous different coordination cages have been, often serendipitously, discovered.

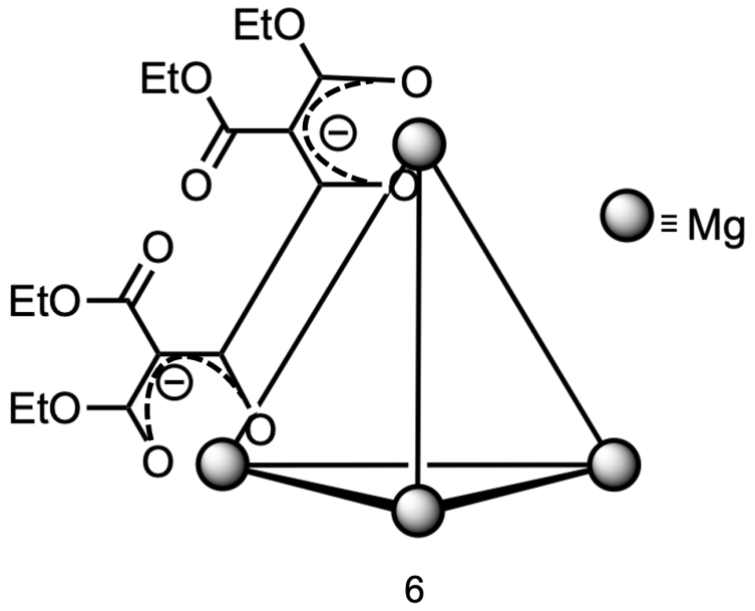

6

Figure 5. The Mg_4L_6 tetrahedron published by Saalfrank et al. in 1988 [12].

The bonds holding a coordination cage together, coordinative bonds (15-60 kcal mol^{-1}), are weaker than covalent bonds (ca. 60−120 kcal mol^{-1}), but stronger than dispersive interactions (ca. 0.5−10 kcal mol^{-1}) [2]. This intermediate bond strength leads to a dynamic system, where bonds can break, and reform and the system can be self-healing. If a bond that does not lead to the most stable structure forms, it will break again, and the assembly process will continue until the most stable structure has formed. This error checking process is highly dependent on the lability of the metals. In order to have an efficient error checking, the kinetics of the ligand exchange reactions need to be fast enough at the temperature used for the assembly. This means that it is much harder to form cages of more inert metals (such as Pt(II)) compared to cages of more labile metals (such as Fe and Co). There are cases where more than one structure has a similar energy, or where certain structures are kinetically trapped. In these cases, the product of the assembly reaction can be a mixture of different species or one single species that is not the thermodynamic product.

The interest in coordination cages initially came from the synthetic challenge of creating the highly symmetric structures. Recently more of the interest has come from the guest binding abilities of coordination cages [1]. The centre of a coordination cage is hollow and can be used to bind guests. The guest binding has been used in many different applications. Some examples include to protect molecules [13], for catalysis [14] and separations [3].

2.2.1 Structure and design of coordination cages

There are coordination cages of many different geometries, structures, and sizes. There are two main factors affecting the structure of a coordination cage [1]. The first one is the metal centre geometry. The metal centres are generally d-block metal ions, for which the d-orbitals are the binding orbitals. Depending on the number of electrons, and which orbitals are filled the metal centres can bind to a different number of ligands, and in different geometries. For example, Fe^{2+} has an octahedral coordination geometry and Pt^{2+} has a square planar geometry. In
Figure 6 the different d-orbital geometries and the electron configurations of Fe^{2+} and Pt^{2+} are presented.

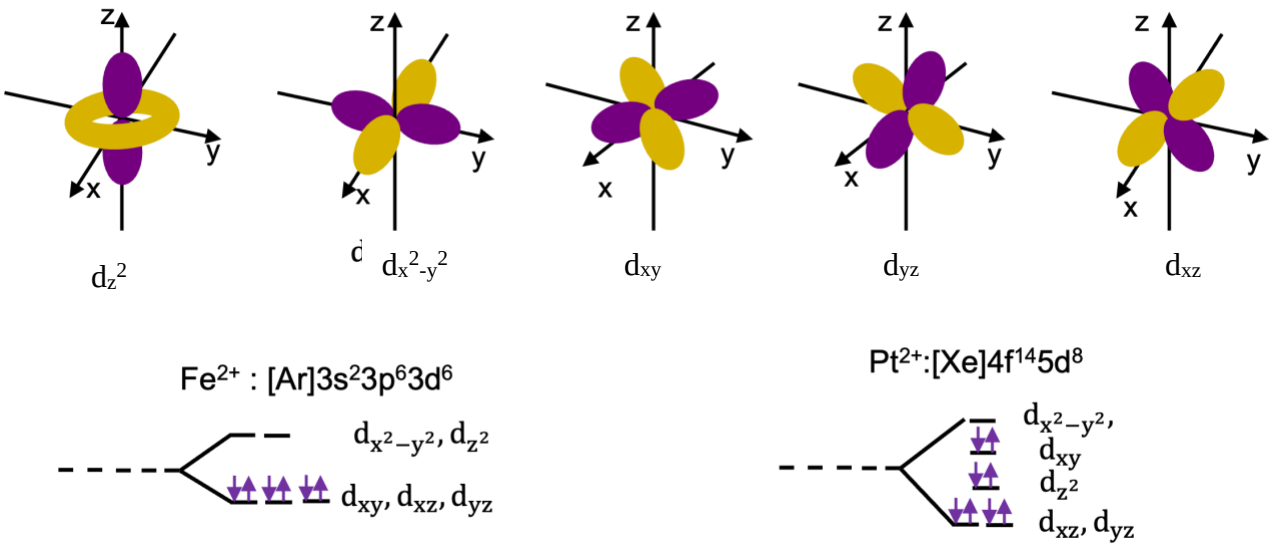

Figure 6. 5 different d-orbitals, and electron configurations of octahedral Fe^{2+} and square planar Pt^{2+}.

The second factor affecting the structure of the cage is the ligand structure [1]. It is the number of coordination sites, the angles between these and their positions that determine the final structure. The ligand can either be edge bridging, as in cages **4** , **5** and **6**, or face capping, like the ligand in cage **7** (Figure 7) [15]. Large, bulky groups of the ligands can also affect what structures a ligand can form.

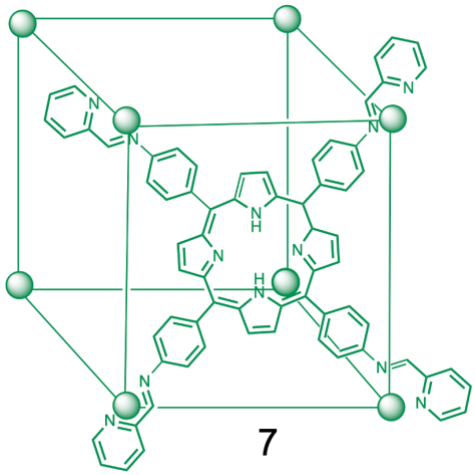

Figure 7. Example of a face-capped coordination cage. The ligands bridge the corners across each face.

To rationally design a coordination cage, the ligands are designed and combined with a metal centre of an appropriate geometry. Often rigid, highly symmetrical ligands are used in combination with metals with a predictable coordination geometry to get a predictable final structure. However, as the

formation of the cage is a self-assembly process governed by the thermodynamics of the system, sometimes the product is unexpected. For example, Zarra et al. combined 4 equivalents of iron(II) with 6 equivalents of a diamine and 12 equivalents of an aldehyde [16]. This combination of ligands and metal centres generally produce tetrahedral cages, but in this case both M_4L_6 tetrahedron **9** and $M_{10}L_{15}$ prism **8** structures were formed depending on the condition (Figure 8).This example highlights the importance and difficulty of design of coordination cages. The cage structure is not only determined by the metals and ligands but also by the solvent used and the assembly temperature. Other factors that can impact the structure of the cage are the presence of guest molecules and the counter ions.

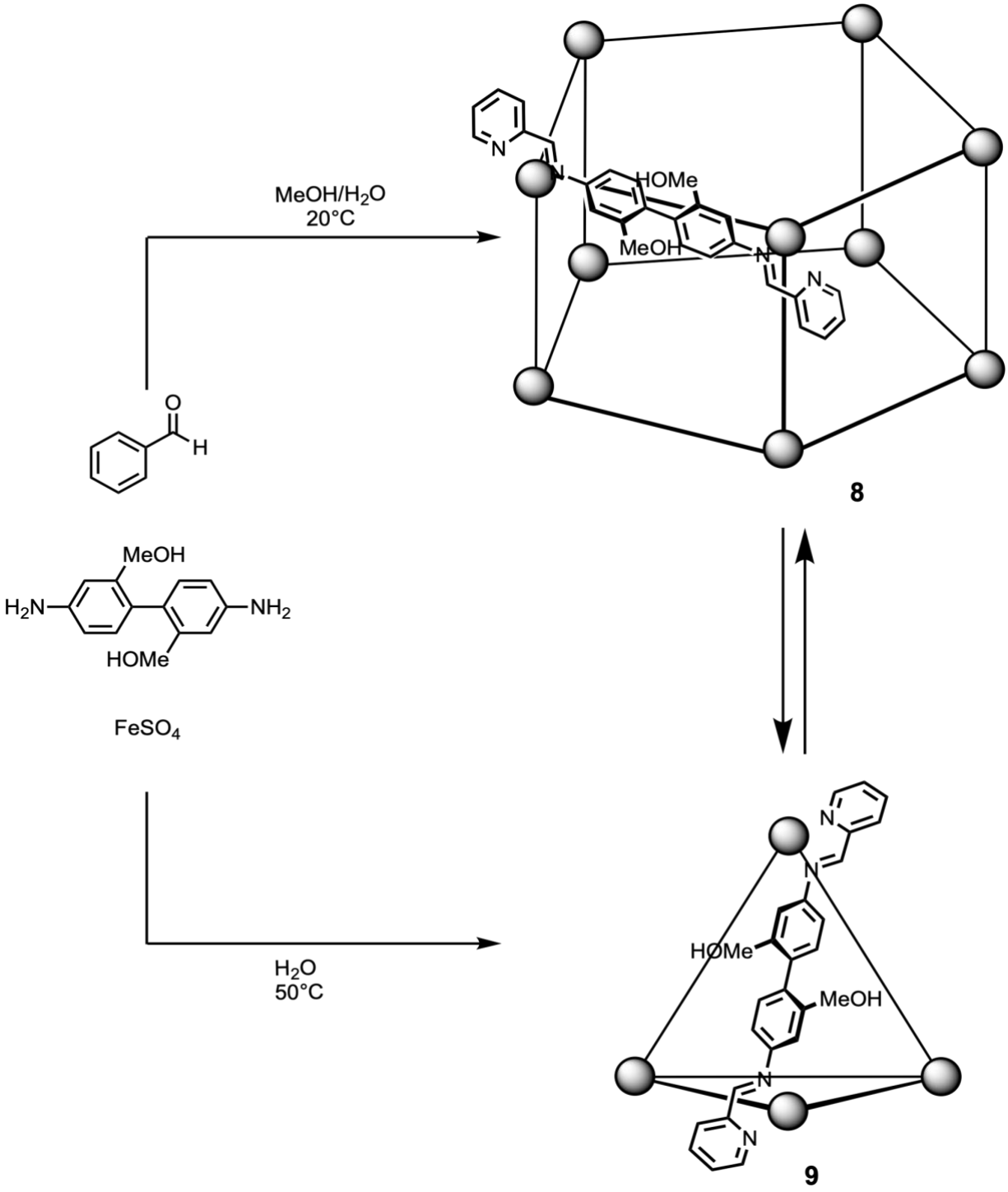

Figure 8. The two cages synthesised by Zarra et al. Depending on the solvent used the product was either a tetrahedron or a prims. The two structures could also be converted to each other.

2.2.2 Formation of coordination cages through subcomponent self-assembly

There are many ways of forming a coordination cage. Common for all of them is that metal ions and ligands are combined and then left to react until the cage has formed. In this work, the cages are constructed in a subcomponent self-assembly reaction. In this process an aldehyde and an amine are combined with the metal ions, and the ligand is formed *in situ* in a templated Schiff base condensation reaction [17]. In this reaction both a coordinative bond (N→M) and a dynamic covalent imine bond (N=C) is formed. By forming the ligand *in situ,* a large increase of complexity is achieved in one single reaction step. The subcomponents are often commercially available or easily synthesized, which reduces the synthesis work needed compared to that of the complex multidentate ligands otherwise used. The cage can also easily be tailored to optimize a specific property by replacing one of the components.

The dynamic nature of the bonds formed in the subcomponent self-assembly reaction means that the structure can be modified after assembly by imine exchange [17]. The dynamic nature also means that there is a built-in error checking process in the assembly of coordination cages. This error checking means that the assembly process continues until the thermodynamically most stable product has formed. The choice of metal ions is very important for the assembly process, and the error checking [1]. The metal centre needs to be somewhat kinetically liable so that wrongly attached ligands can leave and re-attach. One downside of the strategy is that the imine bond can easily be broken under acidic conditions, which makes the cages unstable in acidic environments. However, this acid sensitivity can also be utilized to control the formation and break down of the cage to control guest release [7].

2.2.3 Solubility of coordination cages and the importance of counter ions

Coordination cages, just like normal molecules, have different water solubility depending on the structure. The presence of many large aromatic or aliphatic groups makes the cages less water soluble, while polar groups make them highly soluble in water. For example, tetrahedral cages formed from Fe(II), aldehyde and a ditopic anilines with methoxy (like cage **9**)([16], [18])or SO_3^- (like cage **4**)[7] functionalities are highly soluble in water (Figure 9). When paired with PF_6^- cage **9** is no longer soluble in water, but instead in acetonitrile. Both cage 4 and 9 can be made as SO_4^{2-} salts in water, but the analogue without a solubilizing substituent (cage **10**) cannot. This cage can, however, be brought into water solution by exchanging the counterions for SO_4^{2-}. In water solution it rapidly decomposes.

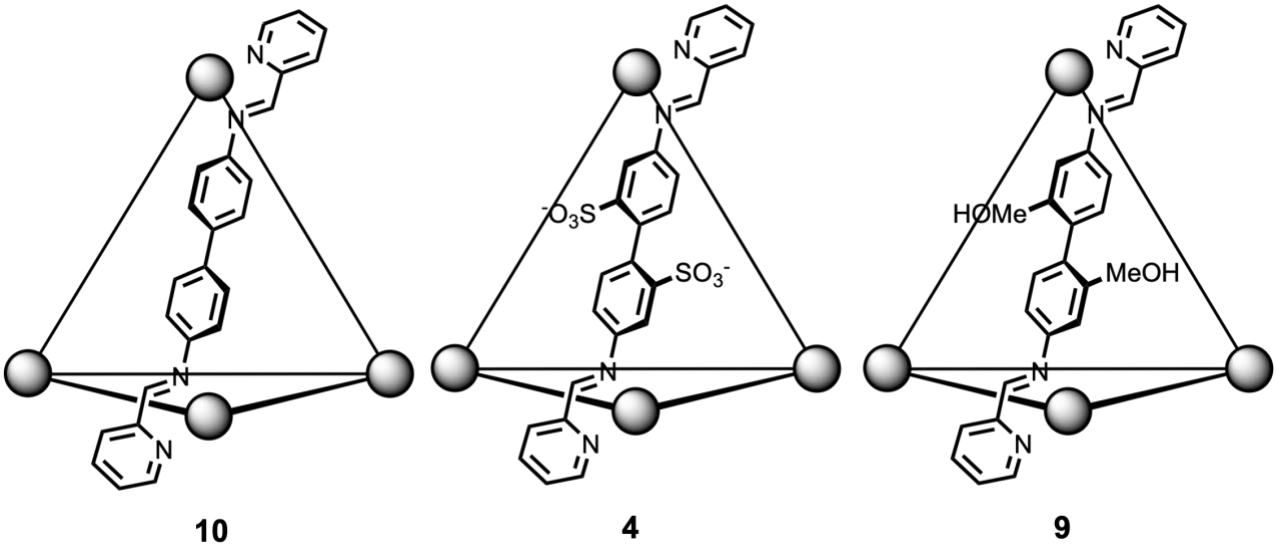

Figure 9. Three tetrahedrons with different water solubilities

In addition to the structure, the solubility of a coordination cage is also dependent on the counter ions the cage is paired with in solution [18]. By exchanging the less hydrophilic triflate ion (OTf^-) for the more hydrophilic SO_4^{2-} ion, several otherwise water insoluble cages become water soluble. This counter ion exchange is reversible, by adding a OTf^- salt the cage could be returned to the original water insoluble form, with over 90% recovery in each anion exchange step.

The counter ion dependent solubility can be used to transfer coordination cages between different phases. The first example of this was reported by Grommet *et al.* in 2017 [19]. They could transport tetrahedron **11** (Figure 10) from water to the ionic liquid 1-hexyl-3-methylimidazolium tetrafluoroborate ([hmim][BF_4]). Cage 11 could also be separated from cage **4** using this phase transfer, as cage **4** does not transfer to the ionic liquid.

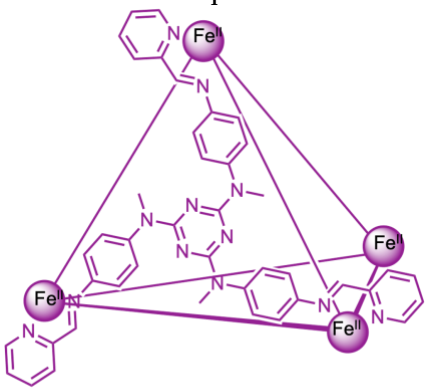

11

Figure 10. Tetrahedral coordination cage that is water soluble as the SO_4^{2-} salt, but that is transported to the hydrophobic ionic liquid [hmim][BF_4]. It can then be isolated as a water insoluble BF_4^- salt.

This phase transfer strategy was further extended to transport cages between water and EtOAc by changing the counter ion, see Figure 11 [8]. By addition of hydrophobic anions (tetrakis(pentafluorophenyl)borate (Li[$B(C_6F_5)_4$])) the cages were transported from the water to EtOAc, and by adding an excess of SO_4^{2-} they could be transported back. This transport back and forth could be repeated up to 11 times without any noticeable fatigue of the system, i.e. without decomposing with the phase transfer cycles. Additionally, it was shown that the phase transfer was selective. When two different cage species were combined the higher charge and lower charge density species transferred first. The phase transfer of the second species did not begin before almost all the first species had transferred.

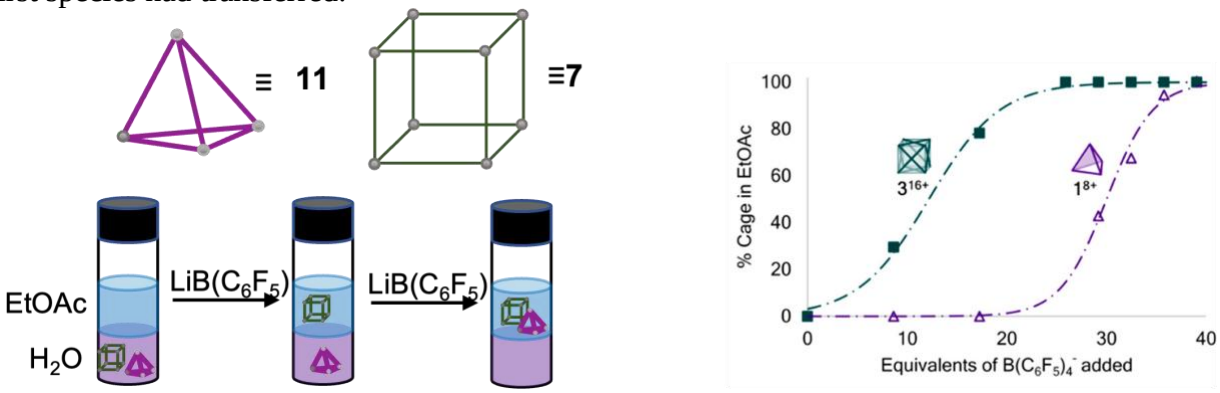

Figure 11. Sequential phase transfer of cages 7 and 11 by addition of a hydrophobic anion. Transfer of 11 does not begin until the transfer of 7 is almost complete. In water the cages are paired with SO_4^{2-} ions.

In addition to the hydrophobicity of the cage the phase transfer also depends on the identity of the counter ion. Coordination cage **12** (Figure 12) could be soluble in three different phases, and it

transferred between the phases in a circular fashion depending on the order in which the counter ions were added [20].

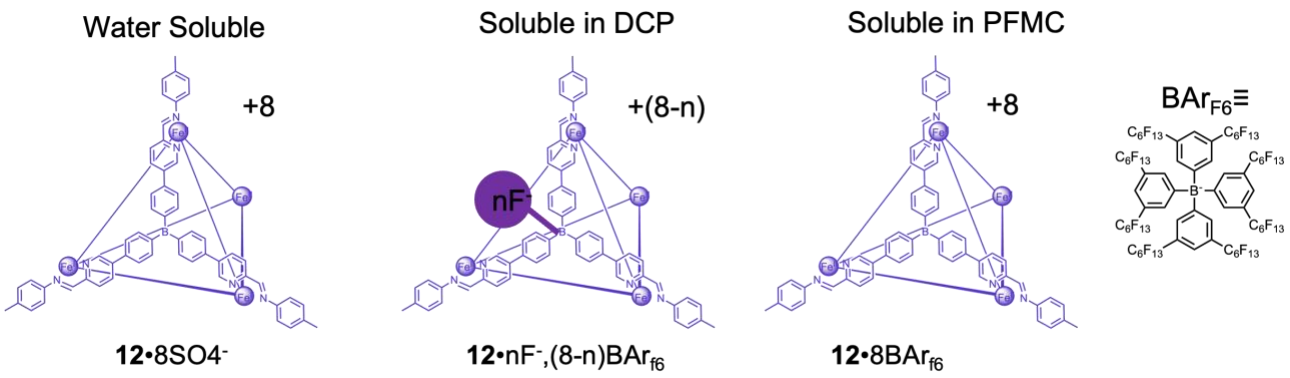

*Figure 12. Cage **12** is soluble in water, 2,2-dichloropropane (DCP) and perfluoromethylcyclohexane (PFMC).*

All examples of phase transfer of coordination cages discussed thus far have concerned cationic cages being transferred by hydrophobic anions. Grancha et al. [21] reported the phase transfer of a hydroxyl-functionalized $Rh(II)_{24}L_{24}$ cuboctahedron **13** (Figure 13), that could be transferred between water and organic solvents (butanol and chloroform) at high pH, when the hydroxyl groups on the cage surface are deprotonated and the cage negatively charged. In this case the phase transfer agent used was cetrimonium bromide (CTAB), a cationic surfactant. This cage is in its neutral form not soluble in water.

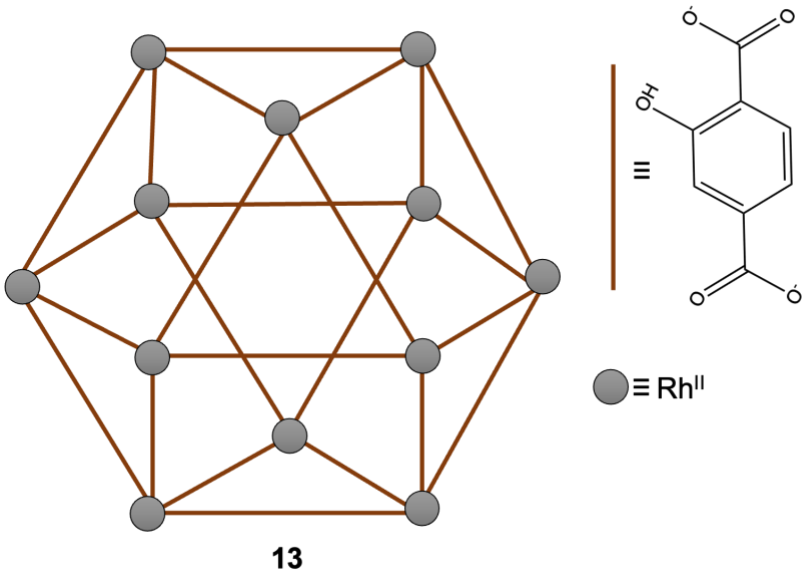

Figure 13. $Rh_{24}L_{24}$ cuboctahedron that can be phase transferred at high pH.

2.3 Heteroleptic coordination cages

One limitation of conventional coordination cages in many applications is the highly symmetric central cavity. A highly symmetric cavity can only bind simple, symmetric substrates, but for many applications more complex substrates are targeted. In nature the low symmetry is very important for the function, of for example proteins [6]. By using multiple types of ligands, forming a heteroleptic coordination cages, a more useful, low symmetry cavity can be obtained[22]. Heteroleptic coordination cages can have more selective guest encapsulation, can encapsulate more complex guests and offer more possibilities for fine tuning the cavity size.

There are two ways to make heteroleptic coordination cages. The first one is to combine multiple ligands (or subcomponents) and metal centres [6]. The other strategy is to combine two different homoleptic cages, and then letting them exchange ligands. When making heteroleptic cages, regardless of the method, there are three possible outcomes (Figure 14). The first one is that the reaction product is a single species, this is called integrative self-sorting. The second possibility is that only the two homoleptic species form, this is called narcissistic self-sorting. The third possibility is that a statistical mixture of species with different combination of the ligands form, this is called social self-sorting [1]. The composition of this mixture will depend on the relative energies of the species in solution.

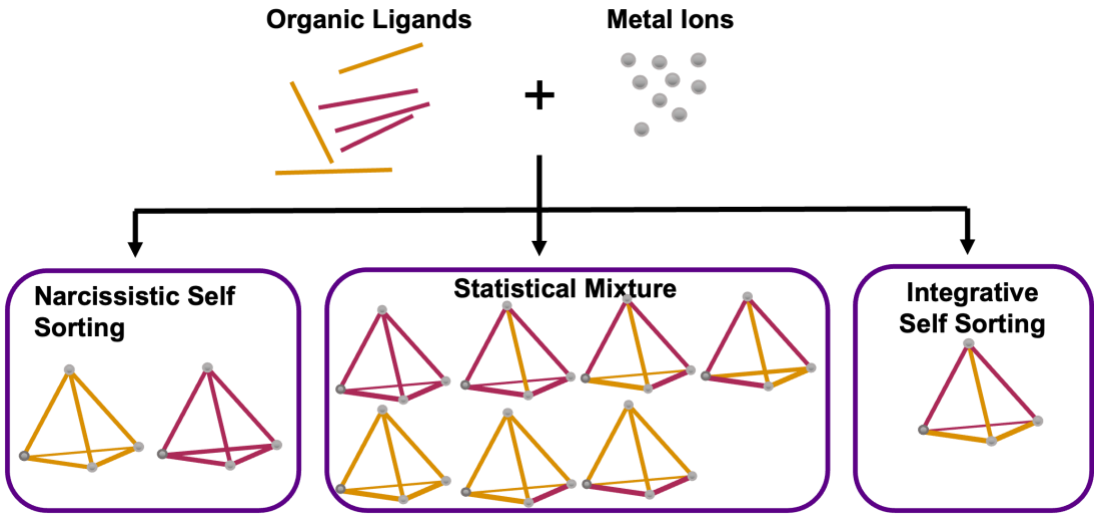

Figure 14. Tthree possible types of products when combining two different types of ligands.

In most cases, only one single species is desired when making a heteroleptic coordination cage. To only get one single product, i.e. integrative self-sorting, the ligands have to fit together like puzzle pieces. This situation, however, is generally entropically unfavourable and therefore difficult to achieve. Therefore, an entropic driving force must be built into the system [22]. There are several strategies that have been used to achieve this, Figure 15 [6]. One is to use a guest to pre-arrange the ligands so that the cage forms in the right structure. The other strategies use interactions between the ligands to make sure only one product forms. These reactions can be geometric (shape complementarity), steric (large substituents in different positions) or electrostatic.

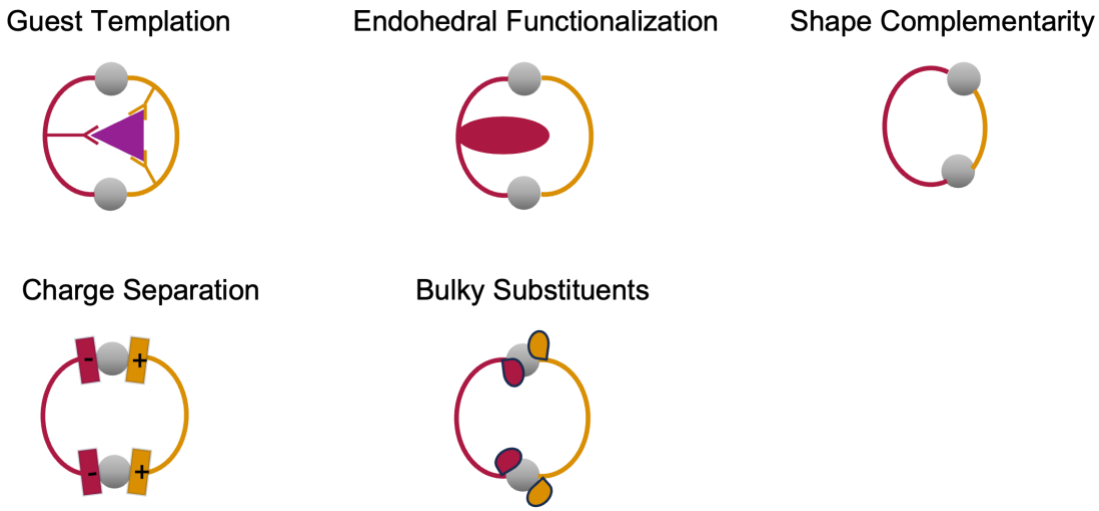

Figure 15. Different strategies to build heteroleptic coordination cages where only one product results from the reaction. Adapted from [6].

Stang et al. were the first to use the strategy of charge separation to form a heteroleptic structure [23]. They combined a ditopic carboxylate ligand (**14**) with a tritopic pyridine ligand (**15**), to form a heteroleptic prism **16** (Figure 16). The driving force for the formation of this cage is the energetic cost of having two ligands with the same charge next to each other. This is an example of destabilizing the homoleptic assembly form a heteroleptic product.

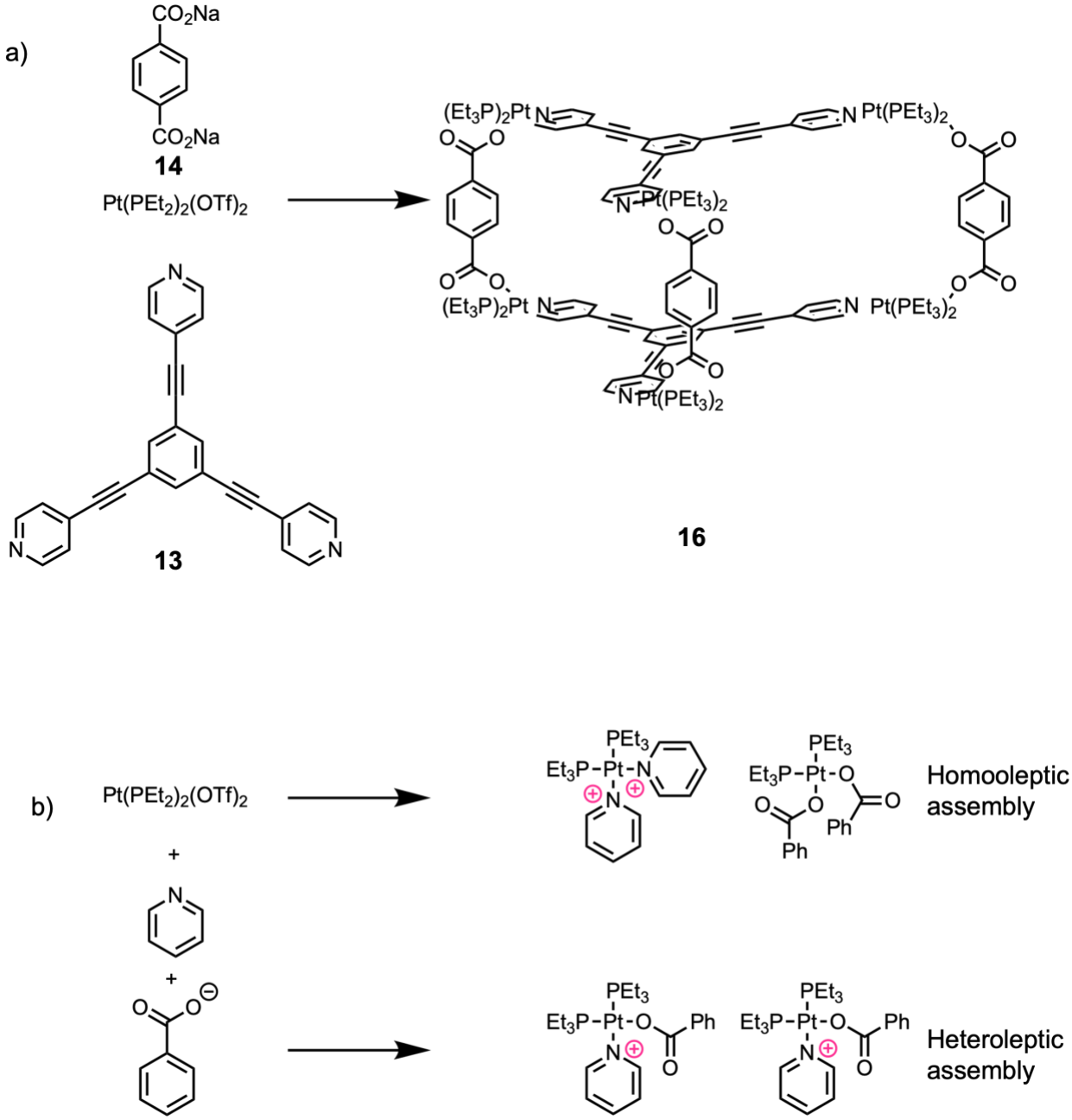

Figure 16. a) Heteroleptic prism formed from a carboxylate ligand and a pyridine ligand [23]. *b) Principle of heteroleptic assembly driven by charge separation.*

Another example of destabilizing the homoleptic form to favour the formation of a heteroleptic structure is the use of bulky ligands that undergo steric clashes in the homoleptic structure. One of the first examples of this was published by Yoshizawa et al. in 2005 [24] (Figure 17). The heteroleptic prism **20** is formed when combining pyridyl ligands **17** and **18** in the presence of guest **19**. The cage did not form without the guest, and with bipyridyl ligands without the sterically clashing methyl groups, the yield was only 60%. More recently the Clever group has successfully formed heteroleptic cages using ligands with bulky substituents, without needing to template on a guest [25], [26]. The Clever group has, also, worked extensively on using and developing different strategies for making

heteroleptic coordination cages based on bidentate banana shaped ligands. For example, they have reported cage **25**, formed using shape complementary ligands **21** and **23 (**Figure 18**)** [27]. As the number of ligands and metal ions increase, it becomes increasingly more difficult to control the formation of the heteroleptic cage and therefore most of the development of new strategies to make heteroleptic coordination cages has focused on small structures [28].

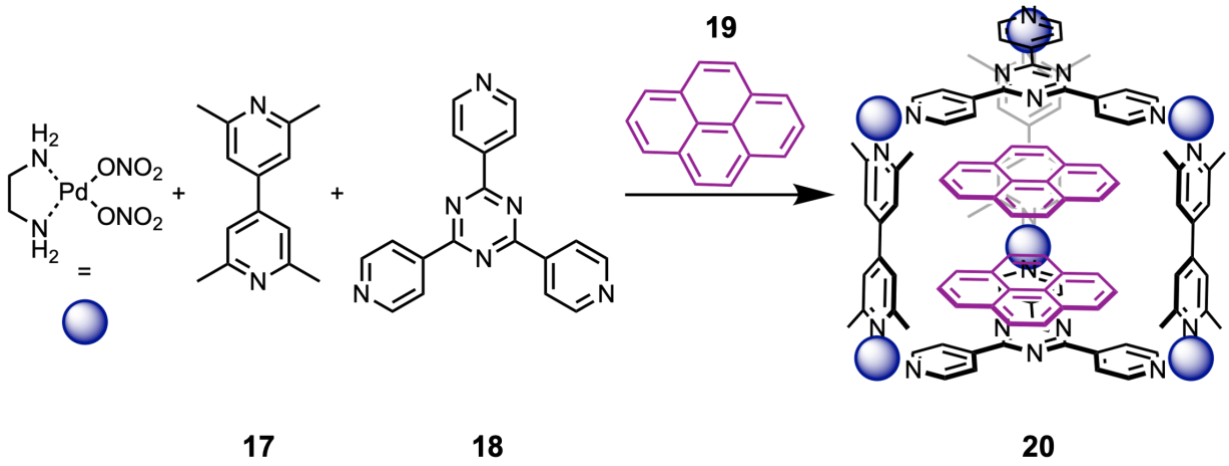

Figure 17. Heteroleptic prism formed using bulky substituents on ligands and guest templating.

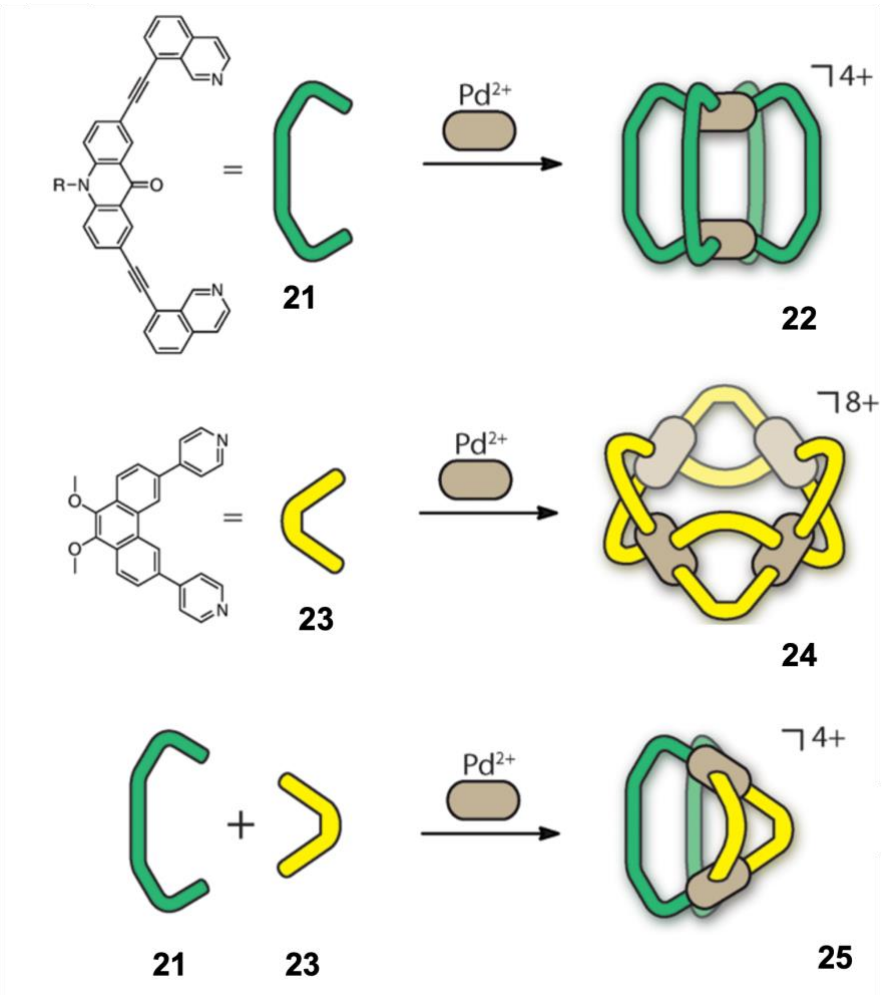

Figure 18. Homoleptic cages 21 and 23 formed from ligands 20 and 22, respectively, and the heteroleptic cage formed integratively when combining the shape complementary ligands Reprinted with permission from [27]. *Copyright 2016 American Chemical Society*[27].

It is also possible to form heteroleptic coordination cages without modifying the system so that there is an enthalpic driving force for the formation of the heteroleptic cage. It is possible to have an entropic driving force for the formation of the heteroleptic cage if the cavity of the heteroleptic structure is smaller than that of the homoleptic structure [29]. Another way is to use kinetic traps, rather than to target a heteroleptic thermodynamic product [30]. This is done by using the strategies described above to increase the energetic barrier for ligand substitution, which can kinetically trap the heteroleptic species.

2.4 Characterization of coordination cages

Different characterization techniques are used to determine the structure of coordination cages, and thus how they can be used in applications. Most of the common molecular characterization techniques, i.e. mass spectrometry (MS), and X-ray crystallography and Nuclear Magnetic Resonance (NMR) spectroscopy, can be used. However, there are some challenges in the characterization of coordination cages due to the supramolecular nature and the presence of metal ions in the structure[1]. X-ray crystallography gives the structure of the cage, but requires the growth of good quality crystals, and it is the solid-state structure that is determined, which is not always the same as the solution structure. NMR gives the number of different ligand environments can be found, which can be used to determine the symmetry of the cage, but it is difficult to completely determine the structure from NMR spectra. Mass spectrometry gives information on the metal to ligand ratio, but no information on how these are organized with respect to each other. Thus, a combination of different techniques is needed to get a complete picture of the structure.

2.4.1 NMR Techniques

NMR spectroscopy is one of the most important characterization techniques used in organic chemistry. Nuclear magnetic resonance is a phenomenon that nuclei with a net spin experience when placed in a static magnetic field and exposed to a second pulsed field [31]. The spin of the nuclei will align with the static magnetic field and when the pulsed magnetic field is on the nuclei are brought out of alignment and will start to rotate about the static field. This rotation is what is detected in the NMR experiment. The frequency of this rotation, called the Larmor frequency or the resonance frequency, is dependent on the magnetic environment of the nucleus. The magnetic environment in turn is dependent on the electron density of the surroundings, when in an external magnetic field electrons will rotate about this field and generate tiny magnetic fields. Different functional groups give rise to different magnetic environments, and the chemical shift can be used to determine the structure of the molecule.

For coordination cages with diamagnetic metals most NMR methods can be used, while it is much more difficult for cages with paramagnetic metals [1]. From the NMR spectra the number of unique ligand environments in the cage can be determined, and from this the symmetry of the cage can be found. ^{1}H and ^{13}C one dimensional NMR are used to identify the cages and any possible break down products. Two-dimensional NMR techniques can be used to study the connectivity of atoms within molecules.

2.4.2 Slice Selective NMR

The resonance frequency of a nucleus in an NMR experiment depends on the strength of a magnetic field [32]. Therefore, a gradient in the magnetic field results in different resonance frequencies along the NMR tube. This is the basis for slice selective NMR, where a gradient field and selection of excitation frequency allows for measurement of only a certain slice. Figure 19 shows a schematic explanation of slice selective NMR. Slice selective NMR has found applications in multi-phase systems [33] and for monitoring of diffusion [32]. In the context of coordination cages, slice selective

NMR has been used to follow phase transfer in-situ [8]. allowing for measurement in the same tube that the phase transfer is performed in. It also allows for identification of the species in the different phases.

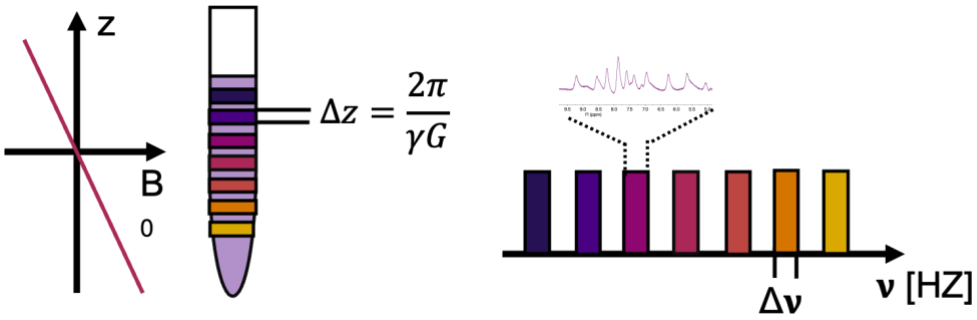

Figure 19. Slice selective NMR uses a gradient in the magnetic field to spread out the NMR resonances of the nuclei along the length of the sample.

The offset the resonance frequency ($\Delta\nu$) experiences at a certain point along the tube can be calculated from Equation 1, where γ is the gyromagnetic ratio of the nucleus, G is the gradient in the magnetic field and z is the vertical deviation from the center of the tube [32].

$$\nu_z = \frac{\gamma G z}{2\pi} \tag{1}$$

The thickness of the slice that is measured (Δz) can be calculated from Equation 2, where $\Delta\nu$ is the bandwidth of the excitation pulse [32]. The offset is usually much larger than the bandwidth used in the experiments, and conventional NMR spectra can be collected for the slices.

$$\Delta z = \frac{2\pi}{\gamma G}\,\Delta\nu \tag{2}$$

2.4.2 Mass Spectrometry

It is difficult to determine the composition (i.e. number of ligands and metal centers) from NMR as NMR only gives information on the number of different chemical environments [1]. X-ray diffraction gives a clear picture of the cage structure but is expensive and requires single crystals. Mass spectrometry offers no geometric information but is a relatively easy way to get information on the number of ligands and metals in the assemblies. Usually, a mass spectrometer with an electrospray ionization is used. Mass spectrometry measurements take place in gas phase and at very low concentrations. This can lead to a different composition than as compared to a much more concentrated solution used in NMR and to breakdown of the cage [1]. Another limitation of mass spectrometry is that the intensity of the peaks does not necessarily correlate to the concentration of the species.

For each coordination cage species there will be a series of peaks corresponding to loss of one counter ion at a time as well as peaks corresponding to fragmentation [1]. This makes the spectra very complex, especially for mixtures of different cages, for instance for a library of heteroleptic coordination cages. It is therefore helpful to separate different species from each other before analysis with mass spectrometry. However, conventional chromatographic techniques cannot be used due to destabilizing interactions between the cage and the stationary phase. Instead, ion mobility mass spectrometry can be used [34]. In this technique the ions are separated based on size and charge before

the measurement. This technique was used in a 2019 publication from the Clever group to resolve minor size differences in a library of heteroleptic coordination cages [34].

3 Results and Discussion

In this chapter the results of the work in this thesis will be presented and discussed. First the structure of new cage 5 is discussed, to evaluate if the heteroleptic library would contain species with a range of cavity sizes. Secondly, the formation of the heteroleptic library is discussed. Lastly the phase transfer of both the anionic homoleptic cage 4 and the heteroleptic cage library is discussed.

3.1 Structure of cage 5

First the two homoleptic cages **4** and **5** were synthesized by combining aldehyde **1** (12 equivalents) and FeSO4 (4 equivalents) with amines **3** and **4** (6 equivalents), respectively, in water (Figure 1). Cage **4** had previously been published, and the NMR spectra of this cage agreed with the literature. Cage **5** is a new cage. Cages formed from similar ligands (for example cages **4**, **10** and **9**) form M_4L_6 tetrahedra, and NMR measurements indicated that cage **5** is consistent what is expected from a tetrahedron (^{1}H-NMR and peak assignment with ^{1}H-^{1}H COSY). Single crystals of the cage were obtained by precipitating the cage from water with PF_6^-, then dissolving it in acetonitrile and slowly diffusing diethyl ether into this solution. To complete the characterization of this new cage a mass spectrum of the cage should be taken. MS measurements of the reaction product in water were unsuccessful. It is known that it is difficult to get cages dissolved in water to fly. Therefore, to further characterize the cage measurements of the cage as a PF_6^- salt dissolved in acetonitrile, and also in a water methanol mixture, which has worked for cage **9** [16].

We hypothesized that cage **5** in water solution will have a conformation different from cage **4**. It is known from previous studies that for cage **4** all the SO_3^- groups are oriented outwards in water solution [7]. This is both to optimize favorable interactions with the water, and to minimize repulsion between the anionic SO_3^-. For cage **5**, however, we think that several of the Me-groups should be oriented towards the center of the cage to minimize unfavorable interactions with the solvent, but due to the limited size of the cavity we did not expect all Me-groups to be oriented endohedrally. To evaluate if this is the case, the three-dimensional structure of cage **5** was constructed using the Python package cgbind [35] (Figure 20). cgbind is built to construct coordination cages from ligands, metal centers and a template from a crystal structure of a cage with the same geometry. However, there are some limitations with the construction of cages done with cgbind. The first one is that the construction of the structure only is based on optimizing ligand-to-metal distances with regards to the template, and to minimize steric clashes. The other limitation is that the cage-solvent interactions are not considered, this is very important for the conformation that a cage adopts, especially in cases where there is some conformational freedom.

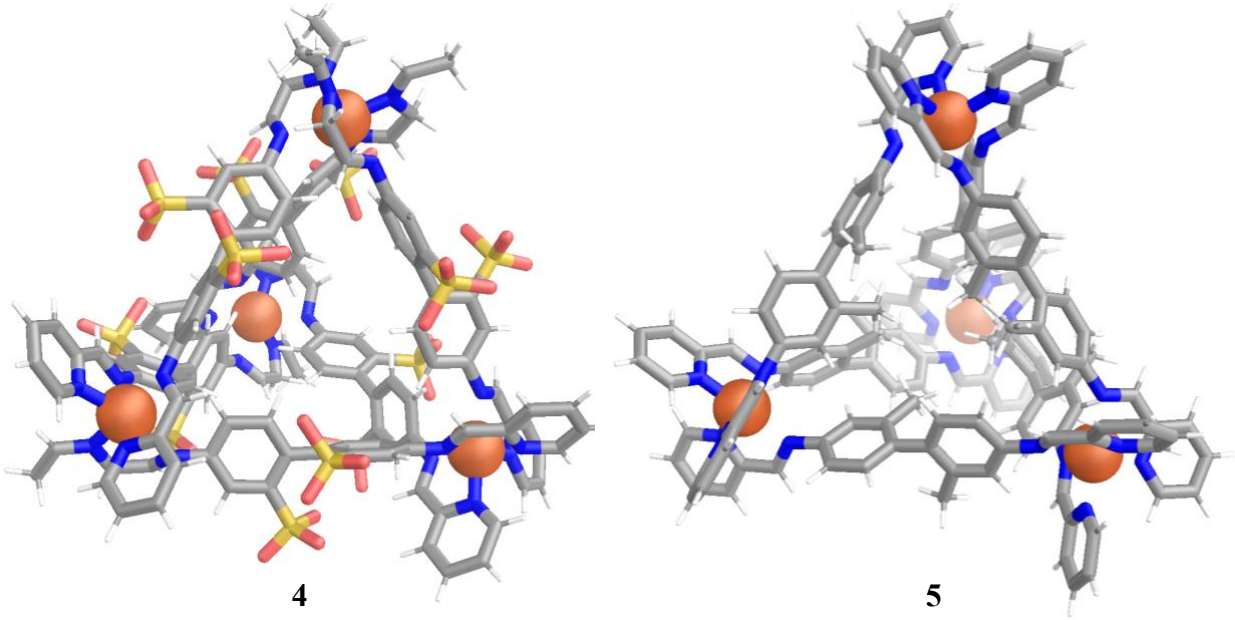

*Figure 20. X-ray crystal structure of cage **4*** [7]. *Cgbind construction of cage **5**.*

If the conformations of the ligand are different, the through space correlations in a NOESY NMR should also be different. Namely, for the conformation of cage **4** there is a through space correlation between the imine hydrogen and the hydrogen next to the substituent group. If both substituents are pointing inwards or in different directions, the correlations should be different. The aromatic region of a NOESY NMR spectrum for cage **5** is presented in Figure 21. For coordination cages, all cross-peaks in the NOESY spectrum generally have the same phase as the diagonal, unlike for small molecules where the cross peaks are in the opposite phase compared to the diagonal. The small unlabeled peaks in the NOESY spectrum are excess aldehyde from the reaction.

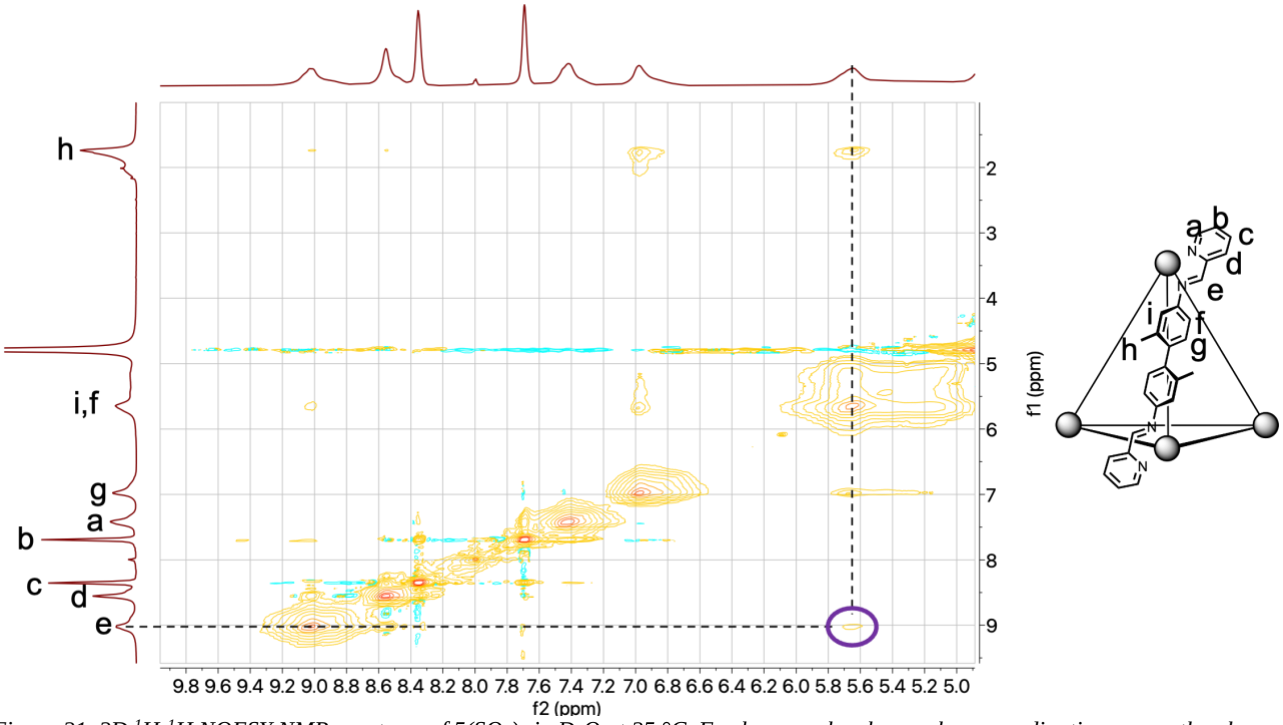

Figure 21. 2D ^{1}H-^{1}H NOESY NMR spectrum of $5(SO_4)_4$ in D_2O at 25 °C. For large molecules, such as coordination cages, the phase of diagonal peaks, NOE cross-peaks and exchange cross- peaks is the same.

In the spectrum in Figure 21 the peaks i and f are not resolved in the spectrum, one or both are correlated to the imine peak. The broad nature of the peak, and the overlap of the two peaks might be due to rotations in the system, or more than one environment for the hydrogens i and f, i.e., if the two rings in the benzidine are not oriented in the same direction. The peak corresponding to the methyl group hydrogens (h) is also very broad and has a big shoulder indicating that the Me-group occupies two distinct chemical environments, likely due to being rotated towards and away from the cavity. The broad nature of the peaks for hydrogens e, i,f and h indicates that the exchange between the two different positions is slow relative to the NMR time scale. If the exchange is fast the peaks only one set of sharp signals would be seen.

To understand better the structure of the cage, X-ray diffraction was performed, see Figure 22. The diffraction was weak, and it was difficult to obtain a complete structure with sufficient data quality, but the structure of the cage could still be made out. The crystal structure confirms the results from the modelling, some of the Me-groups are oriented towards and away from the cavity. This is likely why the peaks for hydrogens i and f in the NMR are not resolved. While the crystal structure is a good tool to get clear information about the structure of a cage, it is not necessarily representative of the solution structure as the diffraction is measured in the solid state at low temperature. There will be more movement in the system in the solution state, and conformations can be solvent dependent. Cage 5 was crystallized from acetonitrile, while the NMR measurements were done in D_2O. As there is likely slow exchange between the conformations in water, the conformation of the cage can adapt to the solvent to optimize its interactions with the solvent. In a more polar solvent than water the methyl groups are probably oriented more towards the cavity, while in a less polar solvent (such as acetonitrile) they will be oriented more outwards, away from the cavity. It would, therefore, be interesting to do NMR measurements of the cage dissolved in acetonitrile, or other solvents to compare.

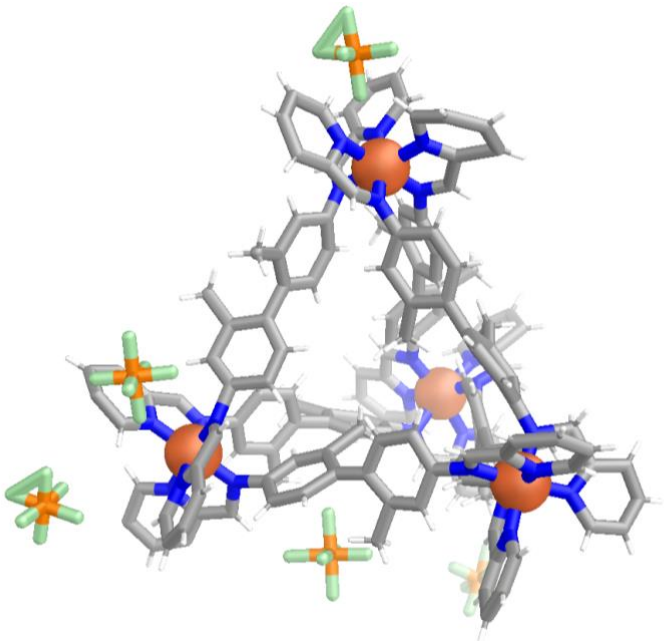

Figure 22. Crystal structure of the tetrahedral cage ***5****[PF_6]$_8$ salt. Some of the methyl groups are oriented towards the cavity, and some away.*

3.2 Synthesis of heteroleptic cage library

Heteroleptic coordination cages can be made in 2 different ways. The first one is to combine the different ligands in the assembly reaction. The second is through ligand exchange, either by combining a homoleptic cage with another type of ligand or by combining two homoleptic cages [6]. If the cages are sufficiently dynamic combining two heteroleptic cages will lead to ligand exchange and formation of heteroleptic cages. To investigate if this was the case for cages **4** and **5**, a 50/50 mixture of the cages was prepared. ^{1}H NMR spectra were taken within a few hours of mixing, after one week and after 1 month (Figure 23). All of the spectra look similar, and like a combination of the ^{1}H NMR spectra of cage **4** and **5**. This means that there is no formation of heteroleptic cages when combining the homoleptic cages at room temperature. It is possible that the cages will scramble at elevated temperatures, and form heteroleptic cages, even if they do not do this at room temperature.

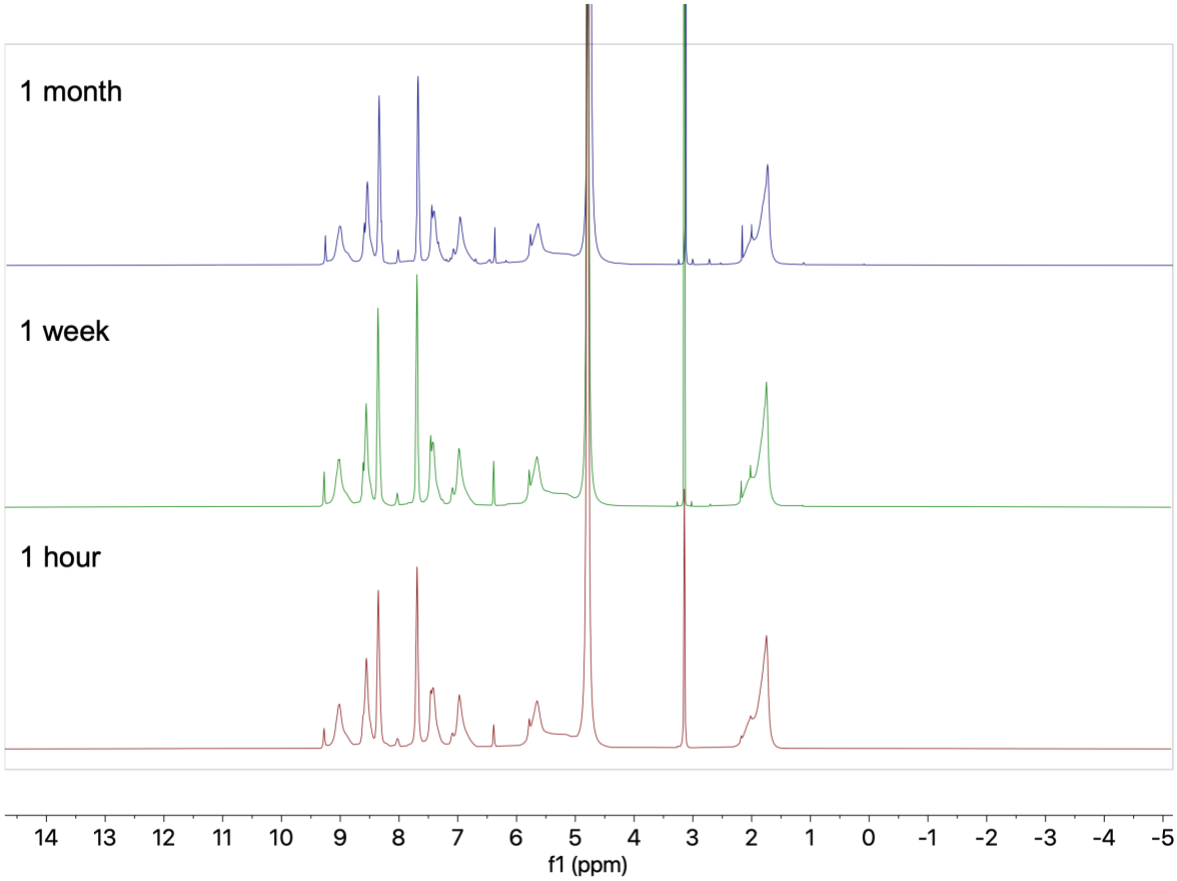

*Figure 23. 1H-NMR spectra of a 50/50 mixture of cages **4** and **5** over time (D_2O, 600 MHz).*

The heteroleptic cage library was synthesized by combining the two amines **2** and **3** (3 equivalents each) with $FeSO_4$ (4 eq), aldehyde **1** (12 eq) and NH_4OH (6 eq). The same protocol used to make the homoleptic cages 4 and 5 was used to make the library. In Figure 24 the 1H NMR spectrum product of this reaction was compared to a 50/50 mixture of the two homoleptic cages. There are more peaks in the spectra of the heteroleptic library sample, compared to a mixture of the two homoleptic cages. Therefore, a library of heteroleptic species has formed., i.e., it is not a narcissistic self-sorting reaction and several different species form. Due to the number of peaks, and the high degree of peak overlap, it is difficult to fully characterize the structures in the library from this NMR spectra. However, based on the discussion in the previous section the high number of different imine peaks (peaks between 9.25 and 8.75 ppm) and peaks around 5.5 ppm there are species with different conformation of the ligands in the library.

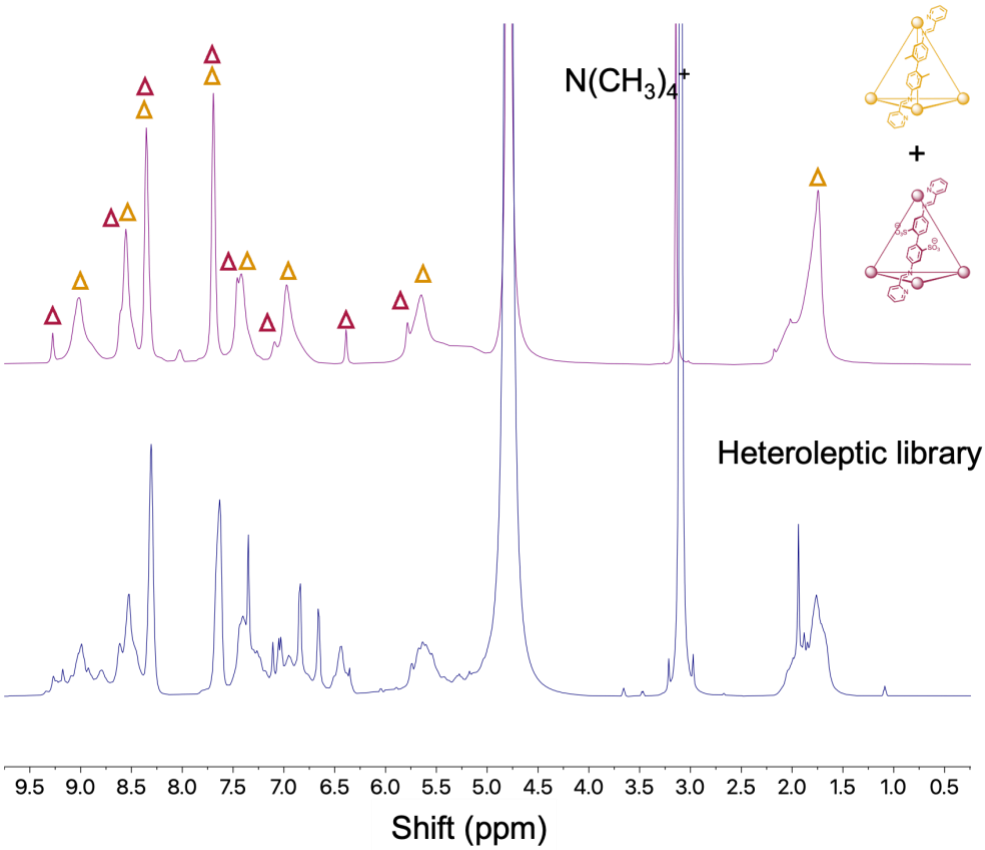

Figure 24. NMR spectra of a 50/50 mixture of the two homoleptic cages 4 and 5 (top) and the heteroleptic library (bottom). Peaks belonging to 4 and 5 are marked with pink and yellow triangles, respectively.

There are six unique chemical environments for the imine hydrogens in the heteroleptic library (Figure 25 a): on Me-ligand on metal center with two other Me-ligands, Me-ligand on metal center with two SO_3^--ligands, on Me-ligand on metal center with one Me-ligand and one SO_3^--ligand, on SO_3^--ligand on metal center with two other SO_3^--ligands, on SO_3^--ligand on metal center with two Me-ligands and on SO_3^--ligand on metal center with one Me-ligand and one SO_3^--ligand. In between these are many smaller signals, probably corresponding to different orientations of the ligands. In the imine region of the NMR spectrum of the heteroleptic library there are 5 distinct peaks (Figure 25 b), and one peak that is very broad. These 5 signals correspond to 5 of the possible configurations, the signal for the last one is likely hidden in the big broad peak, or in the shoulder of the most up field peak. The signal at 9.27 (the most up field signal) corresponds to imine hydrogens at corners where all the neighboring ligands are also SO_3^- ligands. The broad nature of some of the peaks is likely related to rotations of the ligands, like in cage **5**. The combinations of the rotations and the many configurations makes detailed analysis of this region difficult. By using a higher field strength and a longer experiment the resolution would improve, and analysis of the different peaks becomes easier. Then the peaks can be deconvoluted and approximate integrals can be taken to determine the relative ratios of the species.

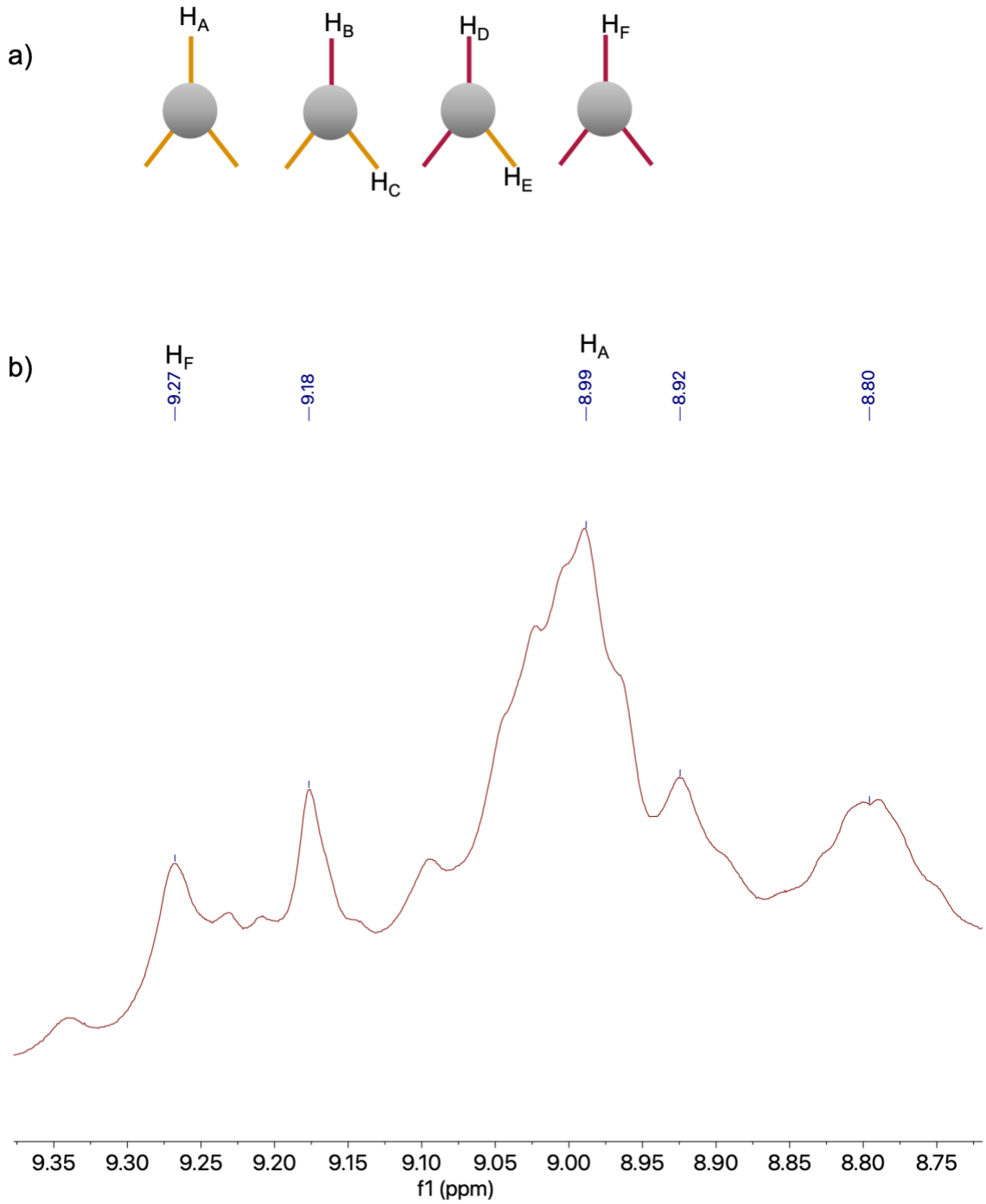

*Figure 25. a) Possible configurations of ligands around iron ions in the heteroleptic cage. Yellow lines correspond to the ligand in homoleptic cage **5**, and red lines correspond to the anionic ligand from cage **4**. b) Zoom in of the aromatic region of the 1H-NMR spectrum of the heteroleptic library. The 5 main peaks are marked and integrated.*

3.3 Initial phase transfer of cage **4**

Anionic homoleptic cage **4** has previously never been successfully phase transferred. Therefore, several solvents and salts were tested. To do this a water solution of cage **4** was combined with an immiscible organic solvent (EtOAc, 1-butanol (ButOH), or chloroform ($CHCl_3$)) in a vial. Small portions of salt where then added, and the vial was shaken to mix the phases. The combinations tested and results obtained are presented in Table 1 and Figure 26. Tetraphenylphosphonium chloride ($P(C_6H_5)_4Cl$) and trihexyltetradecylphosphonium chloride ($P(C_6H_{13})_3(C_{14}H_{29})Cl$) were selected

because of their structural similarity to the hydrophobic anions used to transfer cationic cages. Cetrimonium bromide (CTAB) was selected because it has been used to transfer a Rh(II) metal-organic polyhedral (MOP), a neutral class of coordination cages [21]. This MOP has OH functionalities that can be deprotonated to be made anionic. After CTAB was found to work, at least partially, didecyammonium bromide (DDAB), a quaternary ammonium salt with two long chains was selected because it is more hydrophobic than CTAB.

*Table 1. Results of initial phase transfer tests. Cage **4**[SO_4]$_4$ in water was combined with an immiscible solvent, and then a salt was added in excess.*

Salts	Solvent		
	ButOH	$CHCl_3$	EtOAc
$P(C_6H_{13})_3(C_{14}H_{29})Cl$	No transfer, solution loses color quickly	No transfer	No transfer
$P(C_6H_5)_4Cl$	No transfer	No transfer	No transfer
CTAB	Some transfer, stops about halfway	Some transfer	No transfer
DDAB	Can get complete transfer	No transfer	No transfer

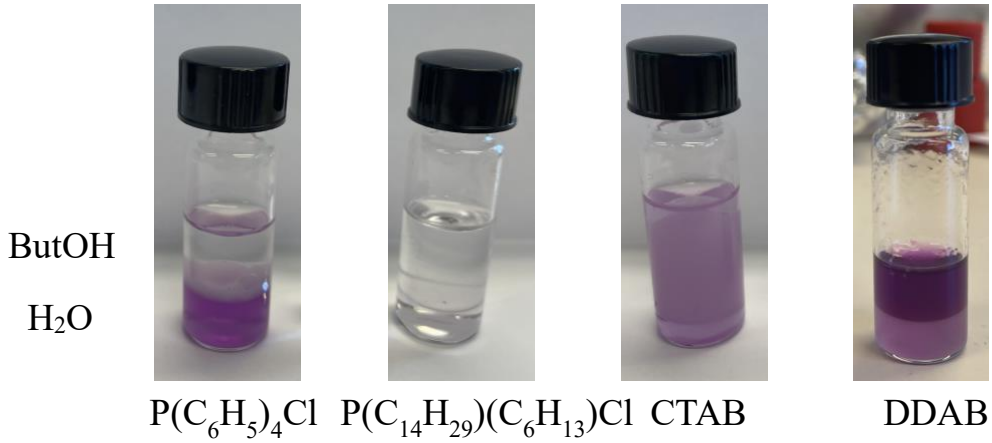

Figure 26. Salts added to a two-phase system of water+cage and ButOH. Photo taken one day after addition of salt, and the cage with $P(C_{14}H_{29})(C_6H_{13})Cl$ had already been broken down.

The two phosphonium salts were not found to work, regardless of the solvent. There are two possible reasons for why the phosphonium salts do not work. The first one is the hydrophobicity of the salts. $P(C_6H_{13})_3(C_{14}H_{29})Cl$ is not miscible with water [36], which means that it is never going to be in contact with the cage. $P(C_6H_5)_4Cl$, on the other hand, is soluble in water, which means that it is not a strong enough phase transfer agent. The other possible explanation is steric interactions. Both the phosphonium salts are bulky with the charge very protected, making strong coordination to the anionic groups on the cage surface difficult.

When $P(C_6H_{13})_3(C_{14}H_{29})Cl$ was added to a system with the cage in water solution and ButOH the solution lost its color within a few hours. This indicates that the cage breaks down, which was later confirmed with NMR. It is difficult to explain the mechanism for this break down. It is possible that some of the cage transferred into the ButOH phase and broke down. Chloride is known to coordinate

strongly with iron (II) and break down iron-based metal centers. However, it was also noted that the cage broke down quickly when transferred to ButOH with CTAB. This could either be caused by the solvent, or the very low concentrations in the organic layer when CTA^+ is used as the phase transfer agent.

For the two quaternary amine salts that did transfer the cage to ButOH, the efficiency was not found to be satisfactory. For CTAB only half of the cage transferred before an equilibrium was reached where no more cage transferred. For DDAB over 100 equivalents was needed to achieve complete transfer, and the cage breaks down rapidly when in ButOH solution. Additionally, it would be better to be able to use the same solvent system to transfer all of the species in the heteroleptic cage library. he solubility of coordination cages formed through subcomponent self-assembly can readily modified by exchanging the aldehyde sub-component [19]. Previously, an aldehyde with a fluorine substituent has been used to increase the hydrophobicity enough to facilitate phase transfers that are difficult to achieve. In this work, cage **27** with 5-methylpyridine-2-carbaldehyde (**26**) as the aldehyde component was synthesized (Figure 27) to increase the hydrophobicity and facilitate phase transfer of the anionic cage. The ^{1}H-NMR spectrum of cage **27** is very similar to that of cage **4**, indicating that the structures of the cages are similar. Peak assignment with ^{1}H-^{1}H COSY confirmed this.

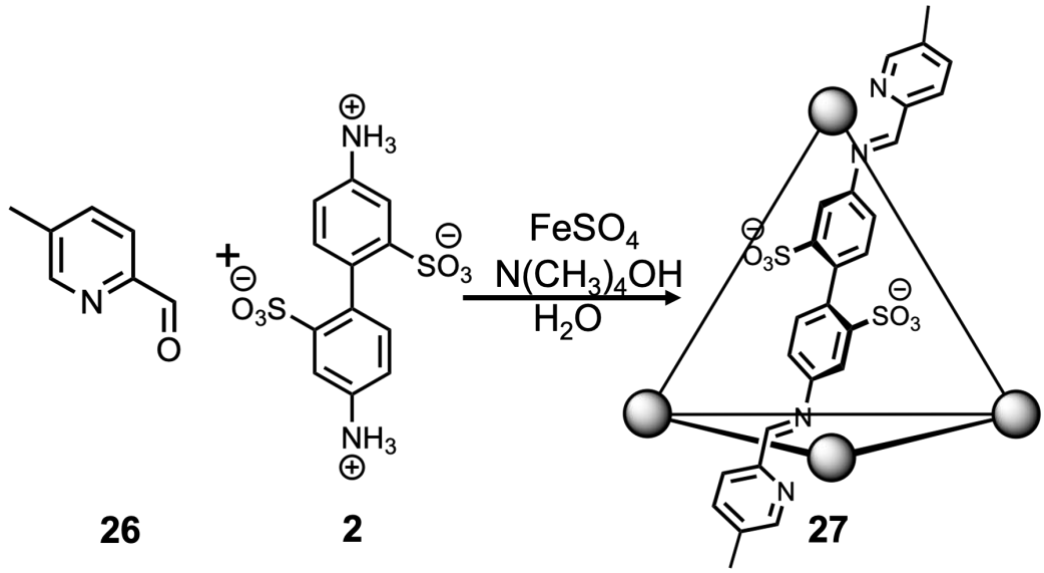

Figure 27. Synthesis of cage with sulfonated ligand and aldehyde component with methyl group. This cage is less water soluable than cage 4.

The phase transfer of cage **27** from water to EtOAc, was investigated by adding a small amount of the salt to a two-phase system, shaking, and letting it settle. It was found that this cage could be transferred to EtOAc with DDAB, but not with any of the other salts used. The complete phase transfer results for this cage are presented Table 2 and Figure 28. No other solvents where tested when EtOAc was found to work, since this would mean that only one organic phase could be used for all transfer steps for the heteroleptic library.

*Table 2. Phase transfer results for transfer of cage **27** to EtOAc.*

$P(C_6H_{13})_3(C_{14}H_{29})Cl$	No transfer
$P(C_6H_5)_4Cl$	No transfer
CTAB	No transfer
DDAB	Transfer

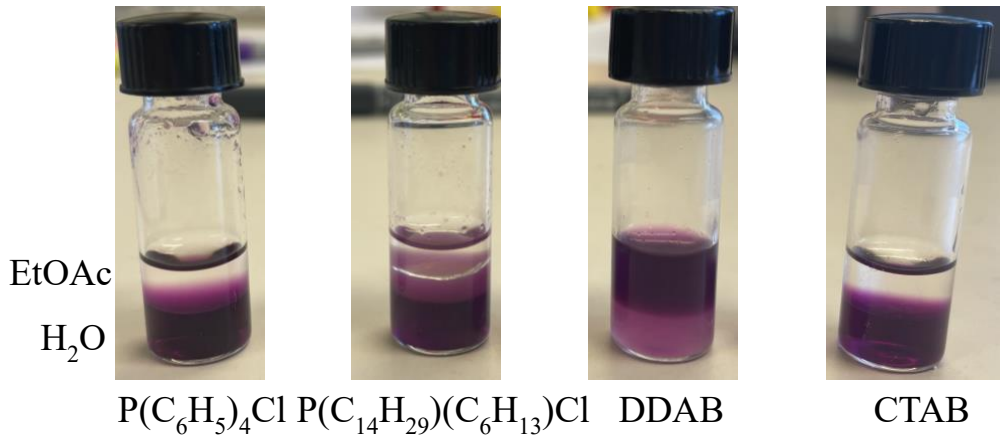

*Figure 28. Phase transfer of cage **27** to EtOAc.*

When the cage **27** in water solution was combined with $P(C_{14}H_{29})(C_6H_{13})_3^+$ in EtOAc, breakdown of the cage was observed. This corresponds to the observation for cage **4** in water combined with ButOH and $(C_{14}H_{29})(C_6H_{13})_3^+$. Therefore, the breakdown of the cage is caused by the salt rather than the solvent. There was a slight discoloration of the EtOAc layer after two days when cage **27** in water solution was combined with $P(C_{14}H_{29})(C_6H_{13})_3^+$ in EtOAc. This could indicate that the cage does transfer but is broken down in the EtOAc layer.

3.3 Phase transfer of cage **5** and a mixture of cages **4** and **5**

Next, the phase transfer of the homoleptic cationic cage **5** was investigated to determine the minimum amount of salt needed to give complete transfer of the cage. This was done to inform the design of the phase transfer of the heteroleptic cage library, specifically to get a sense of how much salt should be added in each transfer step. We were also interested in if the phase transfer of cage **5** would be affected by the presence of cage **4**. It is possible that cage **4** could act as a counter ion to cage **5** and compete with any anions added to the system. To investigate this the phase transfer of a 50/50 mixture of the two cages was followed by slice selective NMR-spectroscopy.

Coordination cages with iron(II) metal centers and bidentate ligands formed in a sub-component self-assembly reaction often have strong colors, in this cage a deep purple color. The phase transfer can, therefore, be followed by UV-Vis spectroscopy. Small portions of a $LiB(C_6F_5)_4$ stock solution were added to a two-phase system with a water solution of cage **5** and EtOAc to determine the minimum amount of salt needed to achieve complete transfer of cage **5**. First a calibration curve was recorded in both the water and EtOAc phases, these calibration curves can be found in the appendix. A stock solution of the cage in water was prepared, at a concentration selected with the help of the calibration curve. 5 mL of the stock solution was added to a centrifuge tube with an equal amount of EtOAc. The salt was added and the tubes were shaken to mix the phases. Aliquots of each phase were taken after the system was left to settle for a short time. In Figure 29 UV-Vis spectra for the phase transfer series and the transfer plot can be found. The phase transfer plot was constructed by fitting the phase transfer data to a logistic function, an S-shaped curve describing the behavior of a dynamic system. The parameters for the fitting can be found in Table 3. The proportion of the cage in each phase was calculated by comparing the initial concentration in the water phase to the transferred amount. If the cage proportion in the phase was found to be smaller than 5%, or if there is no defined peak at the wavelength of maximum adsorption in the higher concentration measurement, the cage proportion is

set to 0. In these cases, scattering due to emulsion formation when the two-phase systems are mixed is measured rather than absorption form the cage.

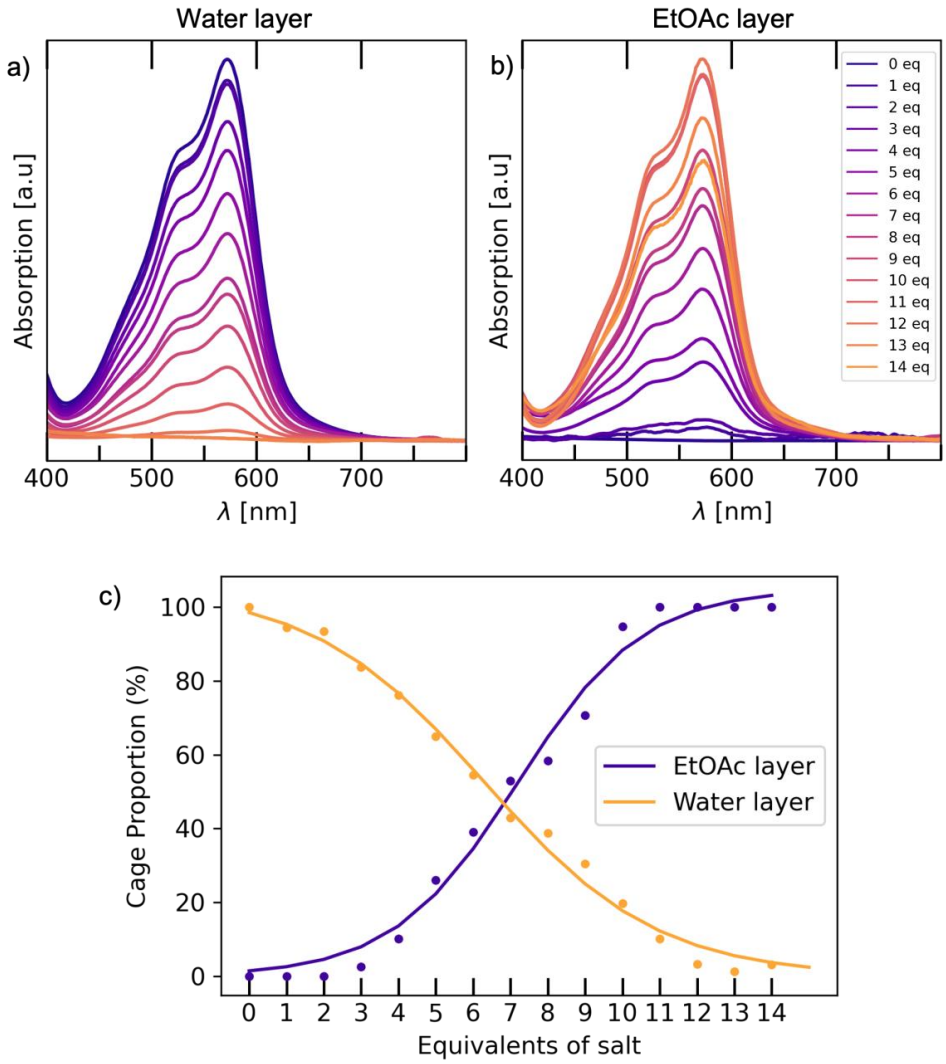

Figure 29. a) UV-Vis spectra of the two phases after addition of salt (0-14 equivalents added in steps of 1). b) Proportion of cage in each layer against equivalents of salt added.

Table 3. Constants (defined according to equation 5.1, see method secction) for the logistic curves fitted to the phase transfer data, and R^2 values for the fits.

Phase	d	L	r	t_m	R^2
Water	0	105	-0.423	6.28	0.95
EtOAc	0	105	0.596	7.20	0.93

The minimum amount salt needed to achieve complete transfer can be found as twice the intersection of the transfer curves for the two phases, at this intersection point approximately 50% of the cage has transferred. This intersection is at around seven equivalents of salt, which means that around 14 equivalents is needed to achieve complete transfer. This is consistent with previous results [8].

As an initial test of the slice selective NMR method for our system, and to determine the effect of cage 4 on the phase transfer of cage 5, a minimum amount of $LiB(C_6F_5)$ was added to a 50/50 mixture

of the two cages. The NMR spectra of this system before and after addition of the salt is presented in Figure 30. When 14 equivalents (to cage **5**) $LiB(C_6F_5)_4$ is added to the two-phase system, all of cage **5** transfer. There are some residual peaks not belonging to cage **4** in thewater layer after the phase transfer, but these peaks likely correspond to aldehyde **1**. Thus, the presence of cage **4** does not seem to significantly affect the phase transfer of cage **5**. There are some peaks in the EtOAc layer after the phase transfer. These peaks do not resemble cage peaks in EtOAc from previous studies, and likely belong to break down products. To confirm this, an NMR of cage **5** in EtOAc should be taken.

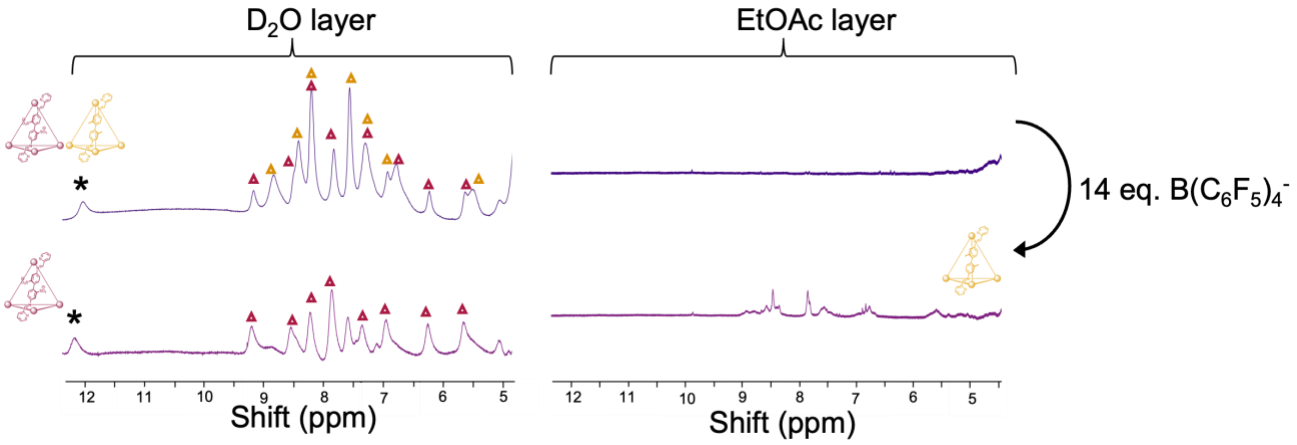

*Figure 30. Phase transfer of cationic cage 5 by addition of LiB(C6F5)4. The cationic cage transferred almost completely after addition of the salt, while the anionic cage 4 remains in the water layer. * denotes peak corresponding to aldehyde component 1, either as a residue from the reaction or from cage break down.*

3.3 Separation of the heteroleptic cage library

The first step towards using phase transfer to separate and isolate species from a heteroleptic cage library was to study the phase transfer behavior of the cage library. This was done as an anion titration, were small aliquots of a $LiB(C_6F_5)_4$ in EtOAc stock solutions were added to an NMR tube containing the heteroleptic cage library in D_2O and EtOAc. In this work, only phase transfer of the cationic cage species in the library was followed due to the difficulty of phase transferring the anionic cages. From these experiments we wanted to see if it was possible to identify different species in the library transferring in a sequential manner, and to determine the amount of transfer salt that should be used in scaled up experiments.

To separate the different species small portions of $LiB(C_6F_5)_4$ was added to an NMR tube containing the heteroleptic library in water solution (about 5mM) and EtOAc in equal amounts. After the addition of the salt the tubes were inverted 10 times and left to settle. The complete NMR data of the phase transfer of the heteroleptic mixture is presented in Figure 31. Only the aromatic region of the slice selective ^{1}H-NMR spectra are shown, because at lower shifts the peaks from the EtOAc completely dominates the spectrum. Due to the low intensity and broad nature of the peaks in the slice selective NMR measurements, it is difficult to completely determine exactly which species are being transferred.

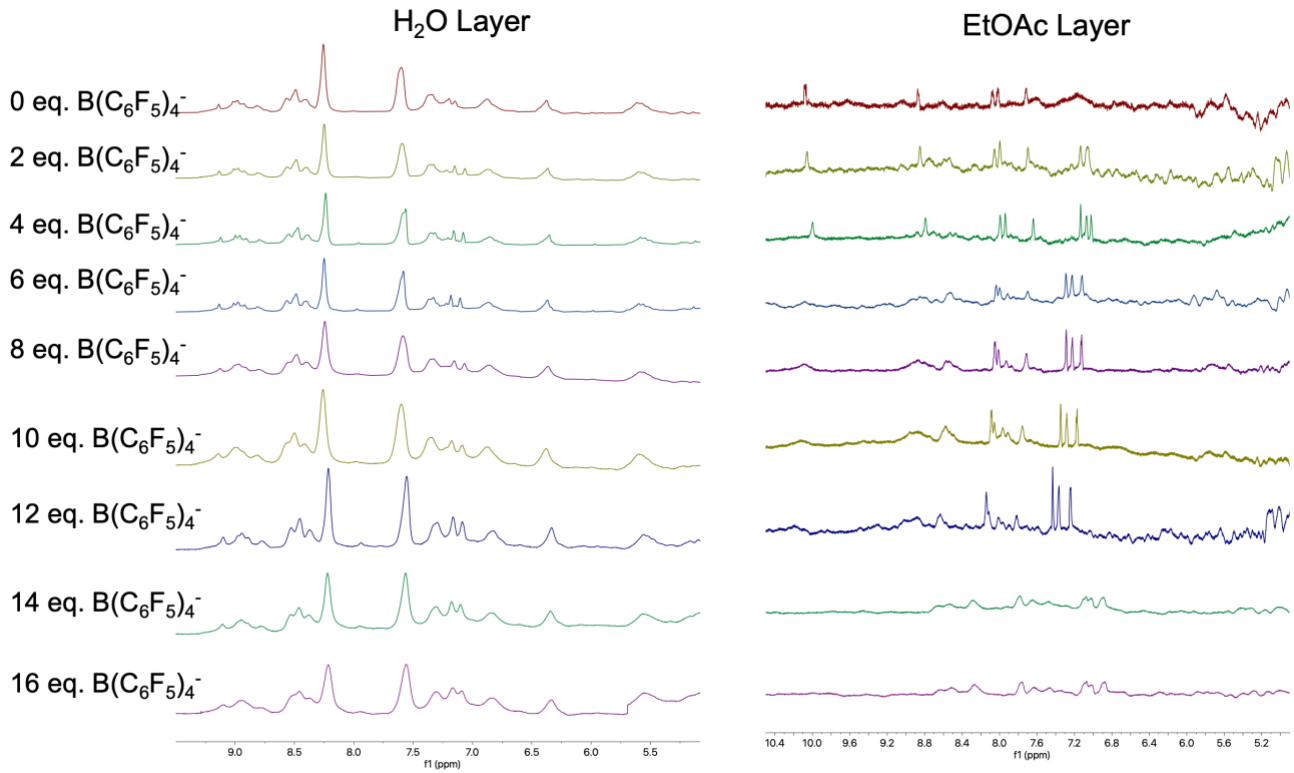

Figure 31. Slice selective NMR spectra for both phases after addition of $LiB(C_6F_5)^-$. The transfer salt was added 2 equivalents at a time.

As more salt is added the number of peaks in the EtOAc layer increases. After 6 equivalents have been added there are 8 peaks in the aromatic region of the EtOAc phase, this indicates that it is a single symmetric species transferring, e.g. cage **5**. As more salt is added the number of species might be increasing, but it is difficult to tell due to the low quality of the data higher salt concentrations. Very high concentrations of salt will introduce extra shielding in the sample and decrease the magnetic field the molecules experience, thus reducing the signal and making it difficult to tune the NMR signal. As there were no problems with the tuning and matching for these samples, it is unlikely that the salt concentration is the main problem.

A more likely explanation is that the settling time between the inversions of the tubes and the measurements was insufficient to achieve good separation of the phases. For a few of the samples it was also difficult to select a good slice. By waiting a longer time, the quality of the data improved (1 week compared to 30 minutes). The problem with this is that the measurements take too long, and that the composition in the phases might change. Different amounts of the two ligands in a phase can lead to changes in the composition of the heteroleptic cage library. There is also the possibility of break down when waiting too long, especially in samples with low concentrations in the EtOAc phase. To avoid very long settling times, an NMR tube centrifuge will be used in future experiments.

3.6 Future work

To complete the characterization of cage **5**, which has not been previously published, it would be good to get a mass spectrum. This was tried, but it was not successful. Getting MS measurements of the cage library would also be a way to characterize the proportion of homoleptic vs. heteroleptic species in the library. It is not possible to get a distribution of the different species directly form the signals in the mass spectrum. Different species might have different fragmentation patterns, and there will be a high degree of overlap between peaks for different species. However, it is possible to compare the in a 50/50 mixture of the cages, and the heteroleptic library at the same concentration of the cages. In this way the fraction of the cages in the library that are homoleptic can be determined

[37]. Using ion mobility mass spectrometry, it would be possible to elucidate the species present in the library without any prior separation. From this MS data, it would be possible to quantify the fraction of the library that is made up of the homoleptic species [34].

In future work, the effects of different cage species on the transfer of others are going to be investigated in more detail. It is known that the presence of other cages can affect the phase transfer [8], and this will likely also be the case for the cages in the system investigated in this report. In this case, the anionic cage could act as a counter ion to the cationic cage and compete with the transfer salt. This would mean that more salt needs to bee added to drive the transfer. To investigate this counterion titrations will be performed with a 50/50 mixture of the two homoleptic cages and followed using UV-Vis spectroscopy. The phase transfer of the heteroleptic library will also be followed by UV-Vis spectroscopy, to see if the transfer of the species in the library does take place in discrete steps. So far this is only an assumption.

The next step towards the new method for synthesis of heteroleptic cages is to characterize the separated fractions. This will be done by first determining the amounts of salt needed to separate each fraction. Salt will be added in small portions until all of one species has transferred. For example, for the first species, about 6 equivalents seem to be needed to achieve complete transfer. When we think that one species has completely transferred the EtOAc layer will be removed using a long cannula needle. Both the water and EtOAc phases will be washed with clean EtOAc and water respectively. After determining the steps needed to take to separate the species, the separation will be done at a larger scale, and the species in the fractions will be characterized by NMR, MS and X-ray diffraction.

NMR spectra of the separated fractions will periodically be taken to determine the changes with time. It is possible that there will be more ligand exchange in the EtOAc layer, where the hydrophobic subcomponents are more soluable compared to in water. It is also possible that there will be a change in the composition of the library when it is dissolved in EtOAc. It is possible that species that are more soluble in EtOAc will dominate, or that more water-soluble species will be precipitated.

Another aspect that would be interesting to investigate is the role of the salt of the hydrophobic counter ion that is used, i.e. if Br^- salts work better than chloride salts. The water solubility of a salt is dependent on the identity of both ions. Additionally, the cage seems to be more compatible with Br^- compared to Cl^-. $P(C_{14}H_{29})(C_6H_{13})_3^+$ might work to do the phase transfer, but it breaks down the cage due to the chloride. It would therefore be interesting to do ion exchange to switch out the counter ion and see if the phase transfer works better. This would also shed light on the steric considerations of the interactions of the hydrophobic counter ion and the cage.

4 Conclusion

Heteroleptic coordination cages are promising materials for biomimetic catalysis, but they are generally difficult to design and synthesize. In this work the first steps towards a novel route for preparation of heteroleptic coordination cages were taken. In this route, instead of targeting a single species, which requires a considerable synthetic effort, a library of heteroleptic species is created and then separated by counter ion induced phase transfer.

To demonstrate this principle a model system with two different ligands of the same geometry was selected. These ligands were formed in situ from an aldehyde component, and two different amine components. When both the amines were combined the product was a library of heteroleptic coordination cages. This library is expected to contain species with a range of different cavity sizes, due to the different optimal conformations of amines 2 and 3. Studies on the homoleptic cage **5** confirmed that this is likely the case. For cage **4** the SO_3^- functionalities are aimed outwards away from the cavity, but the crystal structure of cage **5** showed that the Me functionalities of that cage are oriented in multiple different directions, which is consistent with our NMR data.

The cationic species in the heteroleptic cage library could be transferred to an EtOAc phase using $B(C_6F_5)^-$. The phase transfer was followed by slice selective NMR. The NMR spectra showed that at least one species transferred. However, due to the low concentration of the individual species, it was difficult to determine the identity of them. In future studies, the cages from the separated fractions will be characterized by mass spectrometry, NMR and X-ray crystallography.

This work contains one of the first examples of successful phase transfer of an anionic coordination cage. Previously, only cationic coordination cages and one anionic metal-organic polyhedral which had a negative charge at very low pH have been phase transferred. The anionic cage **4** was difficult to transfer due to the SO_3^- functionalities which renders it too water soluble. This highlights the balance between cage structure and counter ion effects in the solubility of coordination cages. By switching the aldehyde component in this cage for one with a methyl functionality water solubility decreased sufficiently to make phase transfer to EtOAc.

When the anionic cage was combined with a chloride salt of the hydrophobic cation the cage breaks down. This break down is likely caused by coordination between the chloride and the iron at the cage vertices. When working with phase transfer of anionic cages, it is important to consider the salt used and how this can interact with the cage. Metal cations readily coordinate with many different anions, and it is important to find a salt where this coordination is not more favorable than the formation of the cage. This is an additional challenge compared to phase transfer of cationic coordination cages, the anions used to do the transfer are generally too bulky to coordinate well with the metal center.

The method developed in this work is expected to significantly reduce the synthesis work required to form heteroleptic coordination cages, especially with ligands of very similar geometry. Thus, there will be fewer constraints on the heteroleptic coordination cages that can be made. This will make the use of heteroleptic coordination cages in applications, such as catalysis or sensing more available. It will also make the use of heteroleptic coordination cages more accessible to the broader nanoconfinement and chemistry community.

5 Experimental Methods

5.1 General experimental

All solvents and reagents were obtained from commercial sources and used as supplied unless otherwise noted. The water and D_2O used in the synthesis of the cages was degassed in 3 evacuation/N_2 fill cycles before use. 1H and 13C NMR spectra were recorded at 600 MHz using a Bruker Avance NEO spectrometer. Slice-selective and 2-dimensional NMR spectra were recorded at 800 MHz on an Oxford 800 magnet, Bruker Avance III HD spectrometer. NMR shifts are expressed in ppm relative to the water solvent peak or to the external standard tert-butanol (t-BuOH) (δ_H = 1.24 ppm) in a D_2O capillary. All measurements were taken at 298 K. UV-Vis measurements were performed on a Varian Cary 50 UV-Vis spectrophotometer. Linear regression was done using the linregress function from the Python-package SciPy.

5.2 Synthesis of cage **4**

This cage was synthesized following the procedure described in [7]. 2-formylpyridine (0.349 mL, 5.6 mmol), 4,4'-diaminobiphenyl-2,2'-disulfonic acid (15 wt% water, 0.7101 g, 1.79 mmol), iron (II) sulfate heptahydrate (0.3323 g, 1.9 mol) and tetramethylammonium hydroxide heptahydrate (0.6450 g, 5.6 mmol) were combined in a 100 mL round bottom flask containing 25 mL degassed water. The dark purple solution was stirred under nitrogen at 50 °C for 20 h. The solution was removed from the heat and allowed to cool. The product was then isolated as a dark purple solid by precipitation with acetone. ^{1}H NMR (600 MHz, D_2O): δ_H = 9.30 (apparent s,12 H, imine), 8.66 (apparent s,12 H, 3-pyridine), 8.35 (apparent s, 12H, 4-pyridine), 7.71(bs,12H, 5-pyridine), 7.48 (apparent s, 12H, 6-pyridine), 7.08 (apparent s, 12H, 6,6'-benzidine), 6.38 (apparent s, 12H, 3,3'-benzzidine), 5.78 (apparent s, 12H, 5,5'-benzadine), 3.13 (s, $[NMe_4]^+$).

5.3 Synthesis of cage **5**

2-Formylpyridine (17 μL, 0.18 mmol), 2,2'-dimethylbiphenyl-4,4'-diamine (20 g, 94.2 μmol) and iron (II) sulfate heptahydrate (17.5 mg, 62.8 μmol) were combined with 3 mL degassed D_2O in a 4 mL vial. The dark purple solution was stirred under nitrogen at 50 °C for 20 h, to yield a 5.2 mM solution that was used without purification. ^{1}H NMR (600 MHz, D_2O): δ_H = 8.83 (bs, 12 H, imine), 8.39 (apparent singlet, 12 H, 3-pyridine), 8.19 (apparent singlet, 4-pyridine), 7.53 (apparent singlet ,13H, 5-pyridine), 7.25 (apparent s, 13H, 6-pyridine), 6.81 (apparent s, 12H, 6,6'-benzidine), 6.38 (apparent s, 12H, 3,3'-benzidine and 5,5'-benzidine), 1.58 (apparent singlet, 36 H, Me-group).

KPF_6 was added to the solution to precipitate the product as a deep purple solid. This solid was then dissolved in acetonitrile, and crystals of X-ray quality were obtained by slow vapor diffusion of diethyl ether into acetonitrile. A suitable crystal was selected and measured on a XtaLAB Synergy R, HyPix diffractometer. The crystal was kept at 116(9) K during data collection. Using Olex2 [38], the structure was solved with the SHELXT [39] structure solution program using Intrinsic Phasing and refined with the SHELXL [40] refinement package using Least Squares minimisation.

5.4 Synthesis of cage **27**

5-Methylpyridine-2-carbaldehyde (14 mg, 0.16 mmol), 4,4'-diaminobiphenyl-2,2'-disulfonic acid (15 wt% water, 20 mg, 58 μmol), iron (II) sulfate heptahydrate (10.76 g, 38.7 μmol) and tetramethylammonium hydroxide heptahydrate (21 mg, 0.11 μmol) were combined in a 100 mL round bottom flask containing 4 mL degassed D_2O. The dark purple solution was stirred under nitrogen at 50 °C for 20 h. The solution was used without further purification. ^{1}H NMR (600 MHz, D_2O): δ_H = 9.29 (s, 12 H, imine), 8.52 (apparent s, 12 H, 3-pyridine), 8.13(apparent singlet, 4-

pyridine), 7.47 (s, 6H, free 4,4'-diaminobiphenyl-2,2'-disulfonic acid), 7.20 (2 unresolved s, 18H, 6-pyridine and free 4,4'-diaminobiphenyl-2,2'-disulfonic acid), 7.03(unresolved s and d, 18 H, , 6,6'-pyridine and free 4,4'-diaminobiphenyl-2,2'-disulfonic acid), 6.42 (apparent s, 12H, 3,3'-benzzidine), 5.82 (apparent s, 12H, 5,5'-benzadine), 3.10 (s, $[NMe_4]^+$), 2.27 (s, 36H, Me on 5-methylpyridine-2-carbaldehyde).

5.5 Synthesis of heteroleptic cage library

The heteroleptic cage library was synthesized using the same procedure as for the two homoleptic cages. 2-Formylpyridine (18 μL, 0.19 mmol), 4,4'-diaminobiphenyl-2,2'-disulfonic acid (15 wt% water, 18.66 g, 47 μmol), iron (II) sulfate heptahydrate (17.46 g, 62.8 μmol) and tetramethylammonium hydroxide heptahydrate (17.07 mg, 94.2 μmol) were combined with 3 mL degassed D_2O. The dark purple solution was stirred under nitrogen at 50 °C for 20 h, to yield a 5.2 mM solution that was used without purification. ^1H NMR (600 MHz, D_2O): available in appendix. Due to high degree of peak overlap and high number of peaks, peaks are not listed, and no integrals were taken.

5.6 Initial phase transfer experiments

For the anionic cage 4 several solvent-counter ion combinations were qualitatively evaluated. The solvents tested were ethyl acetate (EtOAc), 1-butanol (ButOH) and chloroform ($CHCl_3$). The salts tested were tetraphenylphosphonium, trihexyltetradecylphosphonium, CTAB and DDAB, see Figure 32.

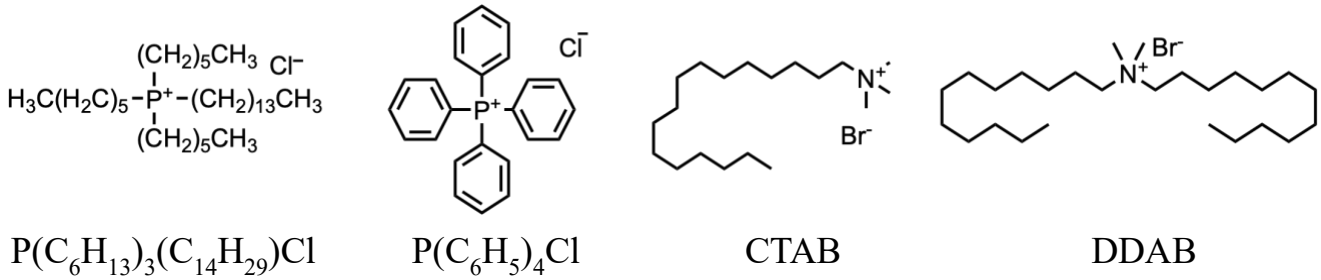

$P(C_6H_{13})_3(C_{14}H_{29})Cl$ $P(C_6H_5)_4Cl$ CTAB DDAB

Figure 32. The salts used in the initial phase transfer evaluation for the anionic cage.

Solutions of cage **4** in water with an approximate concentration of 1 mM were prepared. 1 mL of this solution was added to a vial together with 1 mL of one of the solvents. Then an excess of one of the salts was added. The vial was capped and vigorously shaken for 10 seconds. The system was then left to settle, and the colors of the layers were noted.

5.7 Monitoring phase transfer using UV-Vis

As the initial phase transfer experiments of cage **4** failed and due to time constraints, the monitoring of the phase transfer was only done for the Me cage. To find an appropriate concentration range in which to do the phase transfer, and to be able to quantify the amount of the cage in the two phases, calibration curves for the cage in water and EtOAc were recorded. The solutions with the lowest concentrations were measured first to mitigate the effects of break down and evaporation of solvent, for this reason measurements in EtOAc were done before measurements of the water phase.

5.7.1 Calibration curve in water

In a 25 mL volumetric flask, 200 μmol of the cage solution from the synthesis of the Me cage was diluted with water to make a 31.4 μM stock solution. This solution was then diluted by 4/5 and a UV-

Vis spectra was recorded after each dilution. The absorption was measured for each solution. Then the maximum absorption (λ=572 nm) was plotted against the concentration.

5.7.2 Calibration curve in EtOAc

A minimum amount of $LiB(C_6F_5)_4$ was used to transfer all the cage from 15 ml of a water stock solution with the concentration 26 mM to an equal volume of EtOAc. This EtOAc stock solution was then diluted by 4/5 in a centrifuge tube (total volume 10 mL), and UV-Vis spectra were recorded after each dilution. To minimize evaporation the aliquots were kept in the capped tubes until it was time to do the measurement.

5.7.3 Anion titration

A 30 μM stock solution of the cage in water was prepared. A 1 mM stock solution of $LiB(C_6F_5)_4$ solution in EtOAc was also prepared. In a centrifuge tube 5 mL of the cage stock solution was combined with the salt stock solution (the volume of 1-14 equivalents ranged from 0.15-2.1 mL), then EtOAc was added until the final volume reached 10mL. The tubes were inverted 10 times and then left to settle for a short time before UV-Vis measurements. The two-phase samples were kept in the capped tube until right before the measurement when the aliquots were taken. The EtOAc layers were measured before the water layers, and low concentrations were measured before higher. The measurements were done in this order to minimize the effects of breakdown and evaporation of the solvent.

5.7.8 Fitting of the phase transfer data

The phase transfer data was fitted to a symmetric S-curve described by equation 5.1. L is the asymptotic limit of maximum transport (100%), d is the asymptotic limit of minimum transport (0%), r is the steepness, and t_m is the inflection point. All available data was fitted to a logistic model using logletlab.com, leaving all parameters unspecified. The anion equivalents required for complete transfer were taken as twice amount at the intersection of the two curves. This point is a good approximation of the point where the phase transfer is 50% done.

$$y = \frac{L - d}{1 + e^{-r(t - t_m)}} + d \tag{5.1}$$

5.8 Monitoring phase transfer using slice-selective NMR

Slice selective NMR was preformed using the automation program for collection of slice selective NMR data in [8]. A two-phase system containing the cage in water solution and EtOAc was prepared in a long 5 mm NMR tube (approximately 200 μL of each phase). The tube was then placed in the spinner so that the interface between the layers ended up in the center of the coil. The sample was locked on D_2O and tuned to the ^1H nucleus but left unshimmed.

First a ^1H NMR spectrum with 1 scan, receiver gain 1 and 0 dummy scans to set the parameters for the automation program. Using the sweep width and pulse angle from the initial 1H experiment, a pseudo 2D NMR experiment was run to map the sample along the z-direction. A representative pseudo 2D spectrum is presented in Figure 33. From this spectrum the slices with the most intense peaks in each phase were selected. 1D 1H-NMR spectra of the slices were selected by setting the offset. These 1H-NMR spectra were collected using 128 scans.

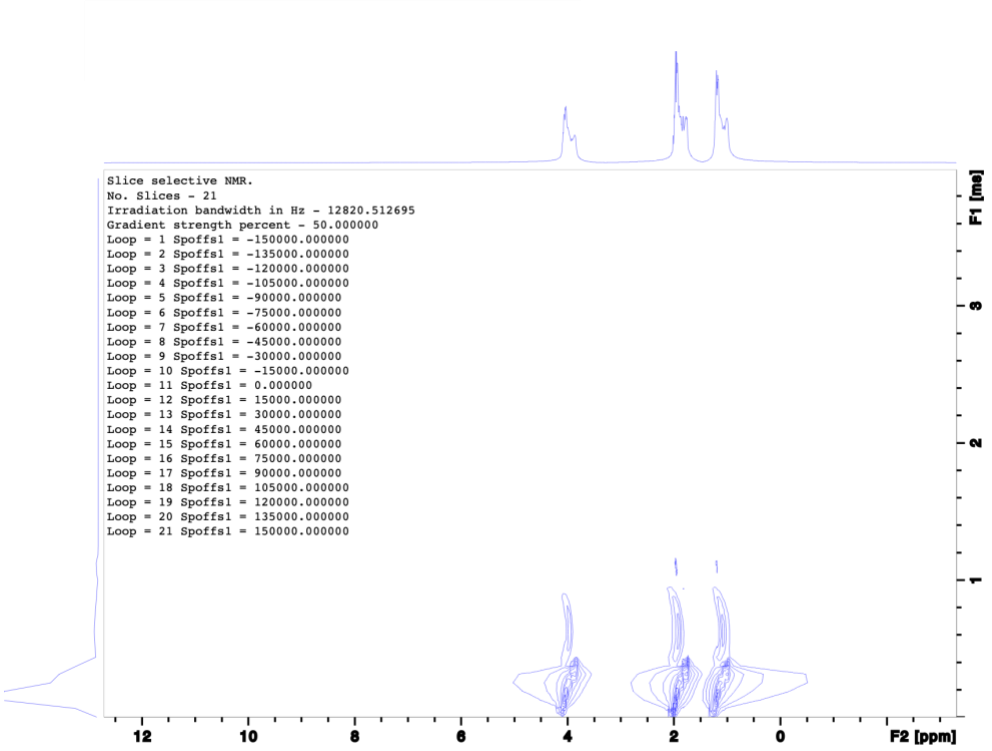

Figure 33. Representative pseudo 2D NMR spectrum for selection of the best slices for slice selective measurements of two-phase system.

To monitor the phase transfer, a 1M $LiB(C_6F_5)$ solution was prepared. This was then added to two-phase NMR sample in portions of 2 µL, which corresponds to around 2 equivalents. After each addition the sample was left to settle for at least 15 minutes, and for up to a week. Then slice-selective ^{1}H-NMR data for both layers was collected using the procedure described above.

References

[1] A. J. McConnell, "Metallosupramolecular cages: from design principles and characterisation techniques to applications," *Chem. Soc. Rev.*, vol. 51, no. 8, pp. 2957–2971, 2022, doi: 10.1039/D1CS01143J.

[2] E. G. Percástegui, T. K. Ronson, and J. R. Nitschke, "Design and Applications of Water-Soluble Coordination Cages," *Chemical Reviews*, vol. 120, no. 24. American Chemical Society, pp. 13480–13544, Dec. 23, 2020. doi: 10.1021/acs.chemrev.0c00672.

[3] D. Zhang, T. K. Ronson, Y. Q. Zou, and J. R. Nitschke, "Metal–organic cages for molecular separations," *Nature Reviews Chemistry 2021 5:3*, vol. 5, no. 3, pp. 168–182, Jan. 2021, doi: 10.1038/s41570-020-00246-1.

[4] Y. Fang *et al.*, "Catalytic reactions within the cavity of coordination cages," *Chem Soc Rev*, vol. 48, no. 17, pp. 4707–4730, Aug. 2019, doi: 10.1039/C9CS00091G.

[5] W. Cullen, M. Cristina Misuraca, C. A. Hunter, N. H. Williams, and M. D. Ward, "Highly efficient catalysis of the Kemp elimination in the cavity of a cubic coordination cage," 2016, doi: 10.1038/NCHEM.2452.

[6] S. Pullen and G. H. Clever, "Mixed-Ligand Metal-Organic Frameworks and Heteroleptic Coordination Cages as Multifunctional Scaffolds - A Comparison," *Acc Chem Res*, vol. 51, no. 12, pp. 3052–3064, Dec. 2018, doi: 10.1021/ACS.ACCOUNTS.8B00415/ASSET/IMAGES/LARGE/AR-2018-004158_0012.JPEG.

[7] P. Mal *et al.*, "An Unlockable–Relockable Iron Cage by Subcomponent Self-Assembly," *Angewandte Chemie International Edition*, vol. 47, no. 43, pp. 8297–8301, Oct. 2008, doi: 10.1002/ANIE.200803066.

[8] A. B. Grommet *et al.*, "Anion Exchange Drives Reversible Phase Transfer of Coordination Cages and Their Cargoes," *J Am Chem Soc*, vol. 140, no. 44, pp. 14770–14776, Nov. 2018, doi: 10.1021/JACS.8B07900/ASSET/IMAGES/LARGE/JA-2018-07900H_0006.JPEG.

[9] J.-M. Lehn, "Supramolecular Chemistry—Scope and Perspectives Molecules, Supermolecules, and Molecular Devices (Nobel Lecture)," *Angewandte Chemie International Edition in English*, vol. 27, no. 1, pp. 89–112, 1988, doi: https://doi.org/10.1002/anie.198800891.

[10] K. Ariga and T. Kunitake, *Supramolecular Chemistry - Fundamentals and Applications: Advanced Textbook*. Springer Berlin Heidelberg, 2006. [Online]. Available: https://books.google.se/books?id=DiXkmgEACAAJ

[11] I. V Kolesnichenko and E. V Anslyn, "Practical applications of supramolecular chemistry," *Chem. Soc. Rev.*, vol. 46, no. 9, pp. 2385–2390, 2017, doi: 10.1039/C7CS00078B.

[12] R. W. Saalfrank, A. Stark, K. Peters, and H. G. von Schnering, "The First 'Adamantoid' Alkaline Earth Metal Chelate Complex: Synthesis, Structure, and Reactivity," *Angewandte Chemie International Edition in English*, vol. 27, no. 6, pp. 851–853, Jun. 1988, doi: https://doi.org/10.1002/anie.198808511.

[13] P. Mal, B. Breiner, K. Rissanen, and J. R. Nitschke, "White Phosphorus Is Air-Stable Within a Self-Assembled Tetrahedral Capsule," *Science (1979)*, vol. 324, no. 5935, pp. 1697–1699, 2009, doi: 10.1126/science.1175313.

[14] Y. Fang *et al.*, "Catalytic reactions within the cavity of coordination cages," *Chem Soc Rev*, vol. 48, no. 17, pp. 4707–4730, 2019, doi: 10.1039/C9CS00091G.

[15] W. Meng *et al.*, "A Self-Assembled M8L6 Cubic Cage that Selectively Encapsulates Large Aromatic Guests," *Angewandte Chemie International Edition*, vol. 50, no. 15, pp. 3479–3483, Apr. 2011, doi: 10.1002/ANIE.201100193.

[16] S. Zarra, J. K. Clegg, and J. R. Nitschke, "Selective Assembly and Disassembly of a Water-Soluble Fe10L15 Prism," *Angewandte Chemie International Edition*, vol. 52, no. 18, pp. 4837–4840, Apr. 2013, doi: https://doi.org/10.1002/anie.201209694.

[17] T. K. Ronson, S. Zarra, S. P. Black, and J. R. Nitschke, "Metal–organic container molecules through subcomponent self-assembly," *Chemical Communications*, vol. 49, no. 25, pp. 2476–2490, Feb. 2013, doi: 10.1039/C2CC36363A.
[18] E. G. Percástegui, J. Mosquera, and J. R. Nitschke, "Anion Exchange Renders Hydrophobic Capsules and Cargoes Water-Soluble," *Angewandte Chemie International Edition*, vol. 56, no. 31, pp. 9136–9140, Jul. 2017, doi: 10.1002/ANIE.201705093.
[19] A. B. Grommet and J. R. Nitschke, "Directed Phase Transfer of an FeII4L4 Cage and Encapsulated Cargo," *J Am Chem Soc*, vol. 139, no. 6, pp. 2176–2179, Feb. 2017, doi: 10.1021/JACS.6B12811/SUPPL_FILE/JA6B12811_SI_002.AVI.
[20] N. Mihara, T. K. Ronson, and J. R. Nitschke, "Different Modes of Anion Response Cause Circulatory Phase Transfer of a Coordination Cage with Controlled Directionality," *Angewandte Chemie International Edition*, vol. 58, no. 36, pp. 12497–12501, Sep. 2019, doi: 10.1002/ANIE.201906644.
[21] T. Grancha *et al.*, "Phase Transfer of Rhodium(II)-Based Metal-Organic Polyhedra Bearing Coordinatively Bound Cargo Enables Molecular Separation," *J Am Chem Soc*, vol. 141, no. 45, pp. 18349–18355, Nov. 2019, doi: 10.1021/JACS.9B10403/SUPPL_FILE/JA9B10403_SI_004.CIF.
[22] C. T. McTernan, J. A. Davies, and J. R. Nitschke, "Beyond Platonic: How to Build Metal-Organic Polyhedra Capable of Binding Low-Symmetry, Information-Rich Molecular Cargoes," *Chem Rev*, vol. 122, no. 11, pp. 10393–10437, Jun. 2022, doi: 10.1021/ACS.CHEMREV.1C00763/ASSET/IMAGES/MEDIUM/CR1C00763_0046.GIF.
[23] Y. R. Zheng *et al.*, "A facile approach toward multicomponent supramolecular structures: Selective self-assembly via charge separation," *J Am Chem Soc*, vol. 132, no. 47, pp. 16873–16882, Dec. 2010, doi: 10.1021/JA106251F/SUPPL_FILE/JA106251F_SI_001.PDF.
[24] M. Yoshizawa, M. Nagao, K. Kumazawa, and M. Fujita, "Side chain-directed complementary cis-coordination of two pyridines on Pd(II): Selective multicomponent assembly of square-, rectangular-, and trigonal prism-shaped molecules," *J Organomet Chem*, vol. 690, no. 23, pp. 5383–5388, Nov. 2005, doi: 10.1016/J.JORGANCHEM.2005.06.022.
[25] R. Zhu, W. M. Bloch, J. J. Holstein, S. Mandal, L. V. Schäfer, and G. H. Clever, "Donor-Site-Directed Rational Assembly of Heteroleptic cis-[Pd2L2L′2] Coordination Cages from Picolyl Ligands," *Chemistry – A European Journal*, vol. 24, no. 49, pp. 12976–12982, Sep. 2018, doi: 10.1002/CHEM.201802188.
[26] B. Chen, S. Horiuchi, J. J. Holstein, J. Tessarolo, and G. H. Clever, "Tunable Fullerene Affinity of Cages, Bowls and Rings Assembled by PdII Coordination Sphere Engineering," *Chemistry – A European Journal*, vol. 25, no. 65, pp. 14921–14927, Nov. 2019, doi: 10.1002/CHEM.201903317.
[27] W. M. Bloch, Y. Abe, J. J. Holstein, C. M. Wandtke, B. Dittrich, and G. H. Clever, "Geometric Complementarity in Assembly and Guest Recognition of a Bent Heteroleptic cis-[Pd2 L A2 L B2] Coordination Cage," *J Am Chem Soc*, vol. 138, no. 41, pp. 13750–13755, Oct. 2016, doi: 10.1021/JACS.6B08694/SUPPL_FILE/JA6B08694_SI_005.CIF.
[28] S. Sudan *et al.*, "Identification of a Heteroleptic Pd6L6L′6Coordination Cage by Screening of a Virtual Combinatorial Library," *J Am Chem Soc*, vol. 143, no. 4, pp. 1773–1778, Feb. 2021, doi: 10.1021/JACS.0C12793/SUPPL_FILE/JA0C12793_SI_002.PDF.
[29] F. J. Rizzuto, J. P. Carpenter, and J. R. Nitschke, "Multisite Binding of Drugs and Natural Products in an Entropically Favorable, Heteroleptic Receptor," *J Am Chem Soc*, vol. 141, no. 22, pp. 9087–9095, Jun. 2019, doi: 10.1021/JACS.9B03776/SUPPL_FILE/JA9B03776_SI_002.ZIP.
[30] D. Preston, J. E. Barnsley, K. C. Gordon, and J. D. Crowley, "Controlled Formation of Heteroleptic [Pd2(La)2(Lb)2]4+ Cages," *J Am Chem Soc*, vol. 138, no. 33, pp. 10578–10585, Aug. 2016, doi: 10.1021/JACS.6B05629/SUPPL_FILE/JA6B05629_SI_002.TXT.

[31] J. Keeler, *Understanding NMR Spectroscopy, 2nd Edition*. 2010.
[32] A.-C. Pöppler, S. Frischkorn, D. Stalke, and M. John, "Toluene and Lithium Amide Diffusion into Polystyrene: A Slice-Selective NMR-Spectroscopic Study," *ChemPhysChem*, vol. 14, no. 13, pp. 3103–3107, Sep. 2013, doi: https://doi.org/10.1002/cphc.201300609.
[33] T. Niklas, D. Stalke, and M. John, "Single-shot titrations and reaction monitoring by slice-selective NMR spectroscopy," *Chemical Communications*, vol. 51, no. 7, pp. 1275–1277, Dec. 2014, doi: 10.1039/C4CC08329F.
[34] K. E. Ebbert *et al.*, "Resolution of minor size differences in a family of heteroleptic coordination cages by trapped ion mobility ESI-MS," *Dalton Transactions*, vol. 48, p. 11070, 2019, doi: 10.1039/c9dt01814j.
[35] T. A. Young, R. Gheorghe, and F. Duarte, "Cgbind: A Python Module and Web App for Automated Metallocage Construction and Host-Guest Characterization," *J Chem Inf Model*, vol. 60, no. 7, pp. 3546–3557, Jul. 2020, doi: 10.1021/ACS.JCIM.0C00519/SUPPL_FILE/CI0C00519_SI_003.ZIP.
[36] M. G. Freire, P. J. Carvalho, R. L. Gardas, L. M. N. B. F. Santos, I. M. Marrucho, and J. A. P. Coutinho, "Solubility of water in tetradecyltrihexylphosphonium-based ionic liquids," *J Chem Eng Data*, vol. 53, no. 10, pp. 2378–2382, Oct. 2008, doi: 10.1021/JE8002805/ASSET/IMAGES/LARGE/JE-2008-002805_0002.JPEG.
[37] F. J. Rizzuto, M. Kieffer, and J. R. Nitschke, "Quantified structural speciation in self-sorted CoII6L4 cage systems," *Chem Sci*, vol. 9, no. 7, pp. 1925–1930, Feb. 2018, doi: 10.1039/C7SC04927G.
[38] O. V. Dolomanov, L. J. Bourhis, R. J. Gildea, J. A. K. Howard, and H. Puschmann, "OLEX2: a complete structure solution, refinement and analysis program," *urn:issn:0021-8898*, vol. 42, no. 2, pp. 339–341, Jan. 2009, doi: 10.1107/S0021889808042726.
[39] G. M. Sheldrick and IUCr, "SHELXT – Integrated space-group and crystal-structure determination," *urn:issn:2053-2733*, vol. 71, no. 1, pp. 3–8, Jan. 2015, doi: 10.1107/S2053273314026370.
[40] G. M. Sheldrick and IUCr, "Crystal structure refinement with SHELXL," *urn:issn:2053-2296*, vol. 71, no. 1, pp. 3–8, Jan. 2015, doi: 10.1107/S2053229614024218.

Appendix

NMR Spectra

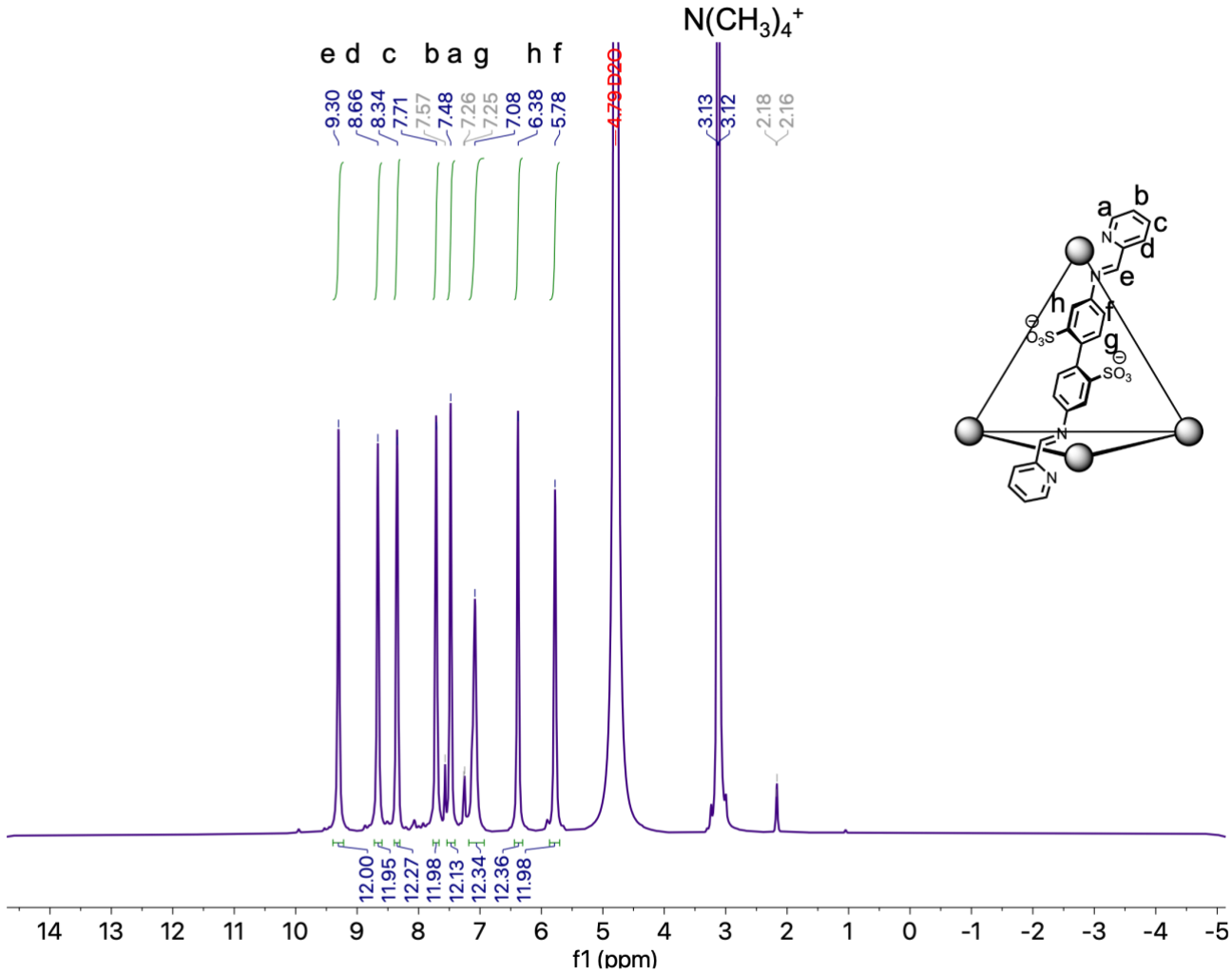

Figure A. 1. ^{1}H-NMR of cage 4[NMe$_4$]$_4$ in D$_2$O, measured at 600 MHz. Small unlabeled signals correspond to excess aldehyde and amine.

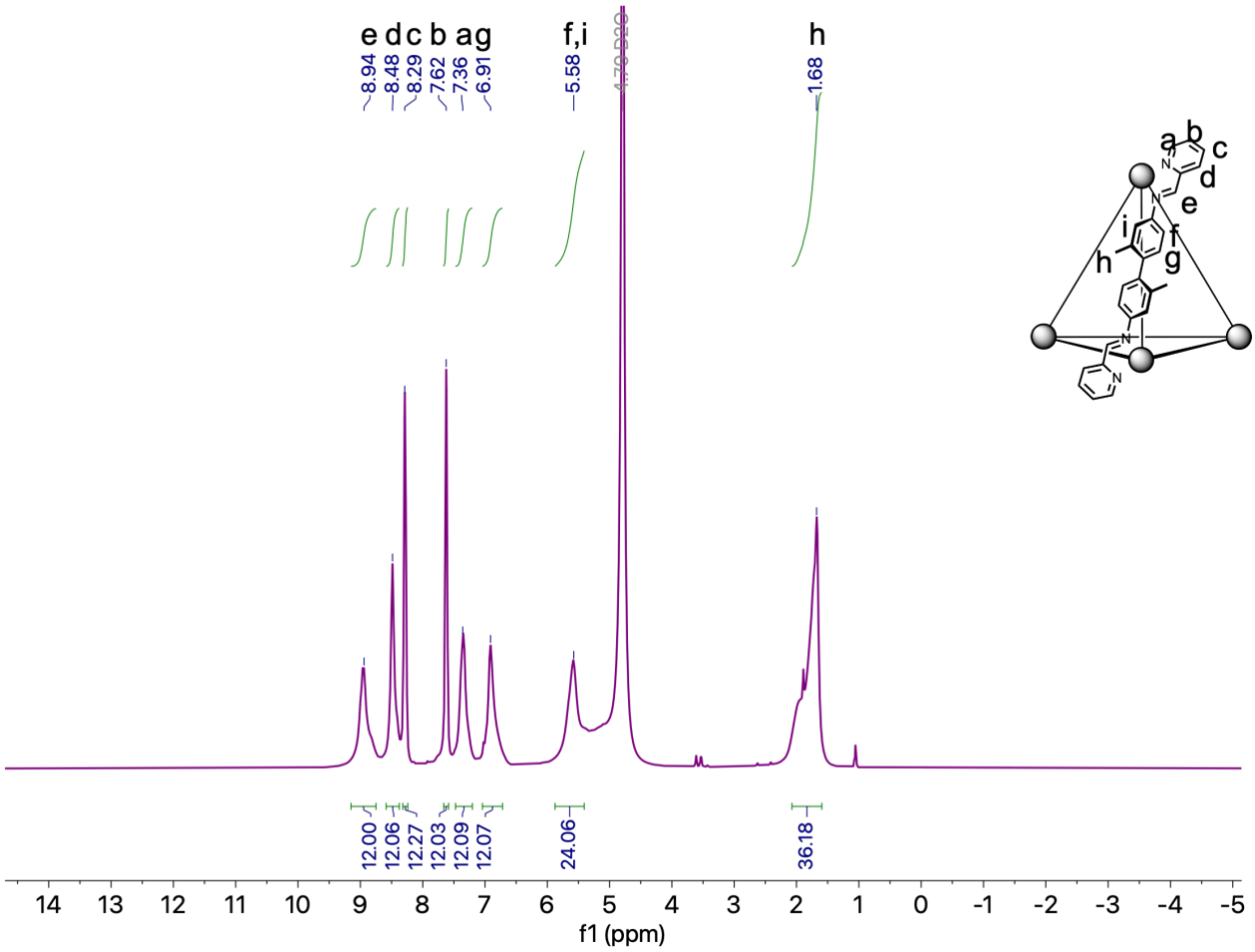

Figure A. 2. 1H-NMR spectra of cage 5[SO_4]$_4$ in D_2O, measured at 600 MHz.

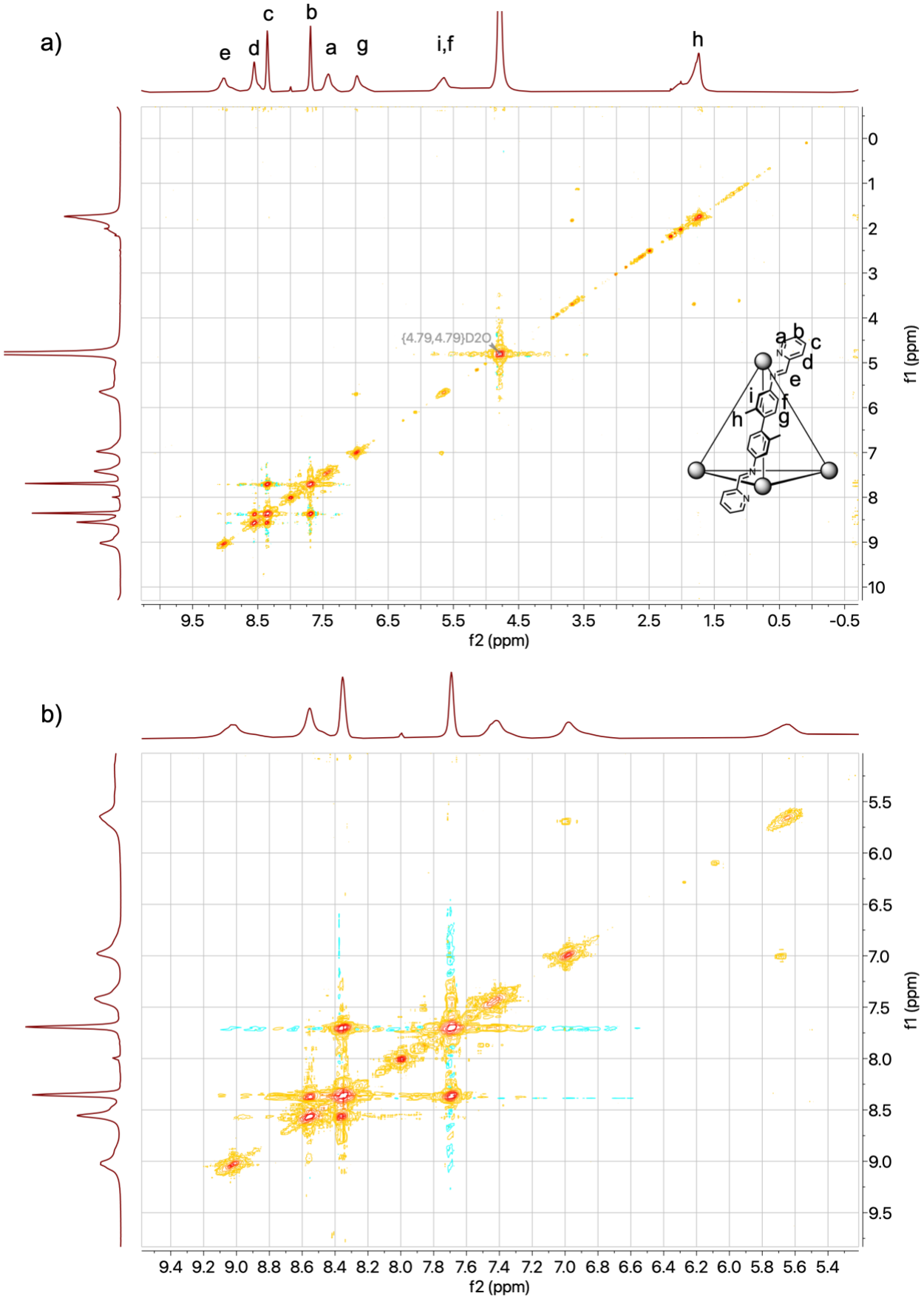

*Figure A. 3. Full ^{1}H-^{1}H COSY spectrum for cage **5**$[SO_4]_4$ in D_2O, measured at 800 MHz.. B) Zoom in of aromatic region of the COSY spectrum of cage 5.*

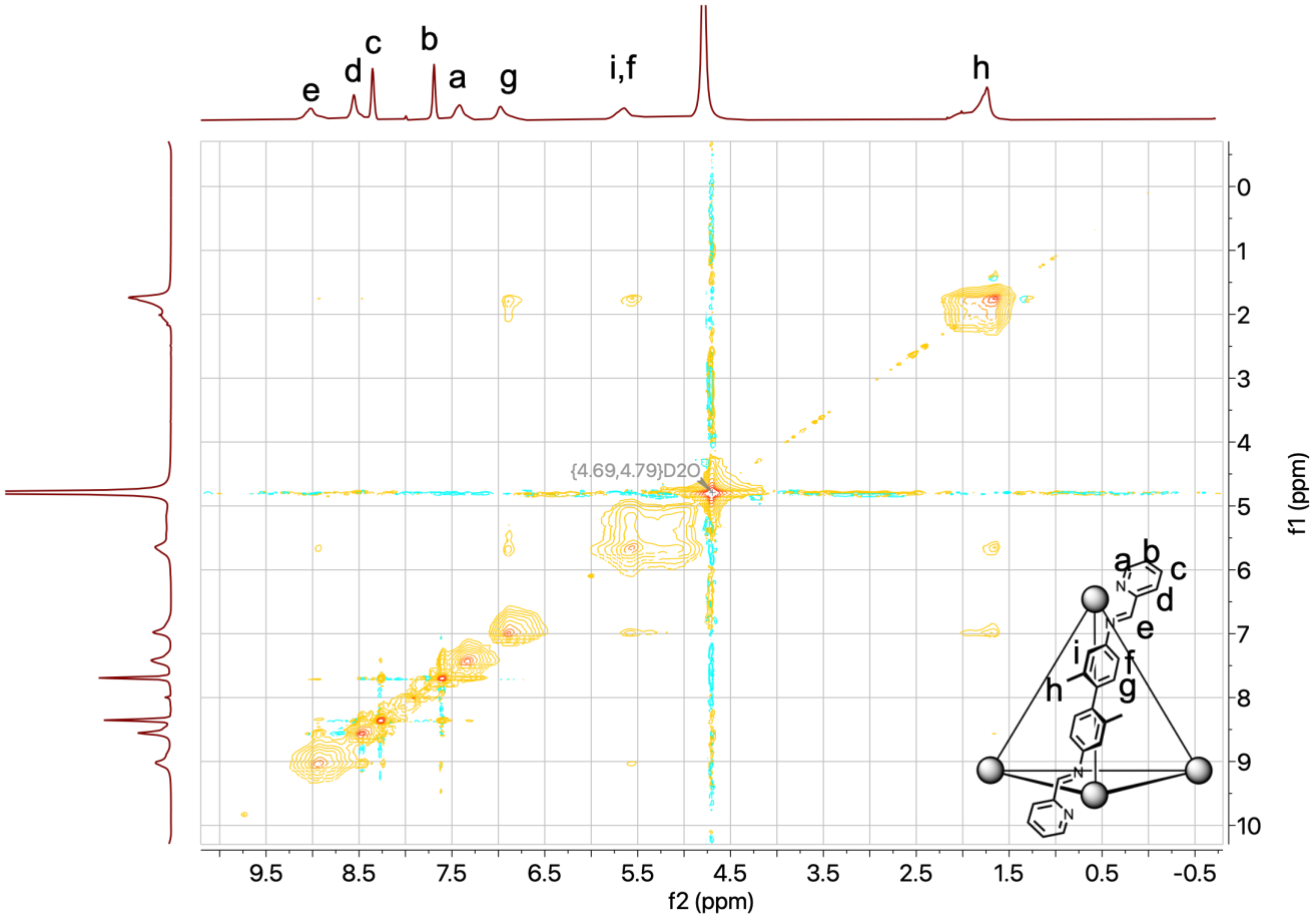

Figure A. 4. ^{1}H-^{1}H NOESY NMR spectrum of 5·$(SO_4)_4$ in D_2O, measured at 800 MHz.

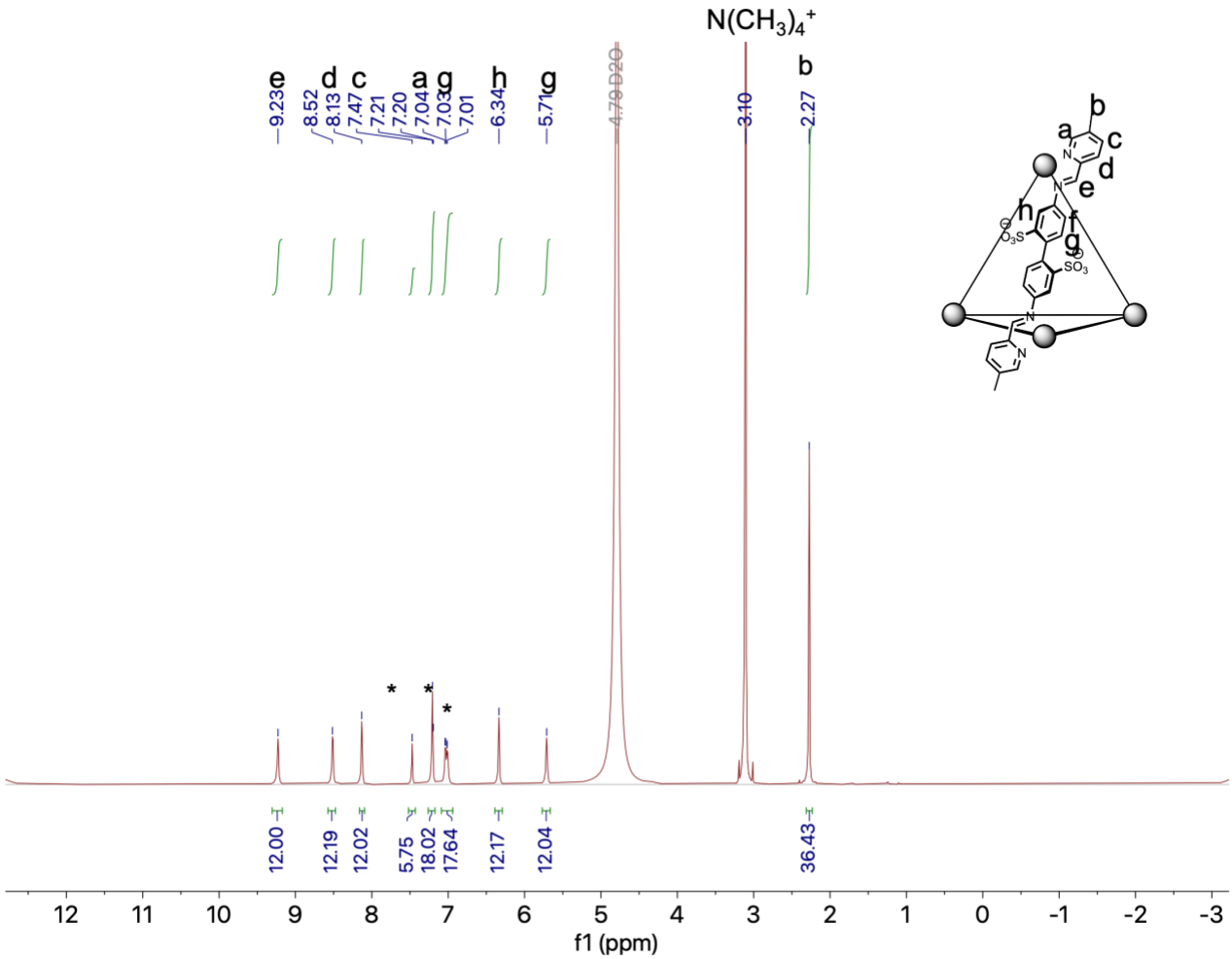

*Figure A. 5. 1H NMR spectrum of cage 27 in D2O, measured at 800 mHz. Peaks denoted with * correspond to excess amine.*

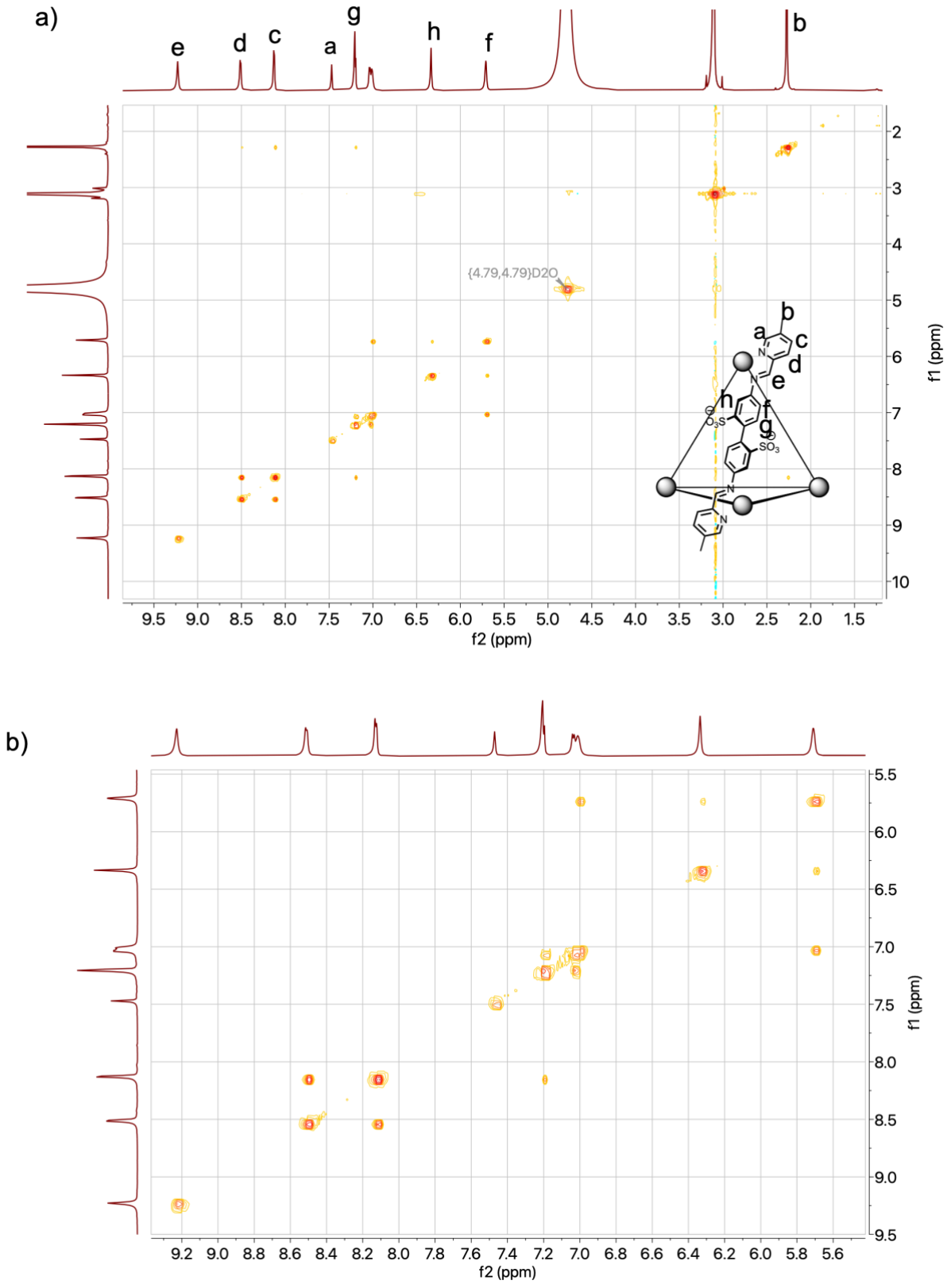

*Figure A. 6. ^{1}H-^{1}H COSY NMR spectrum for cage **27** in D2O, measured at 800 MHz. a) full spectrum b) Zoom in of aromatic region.*

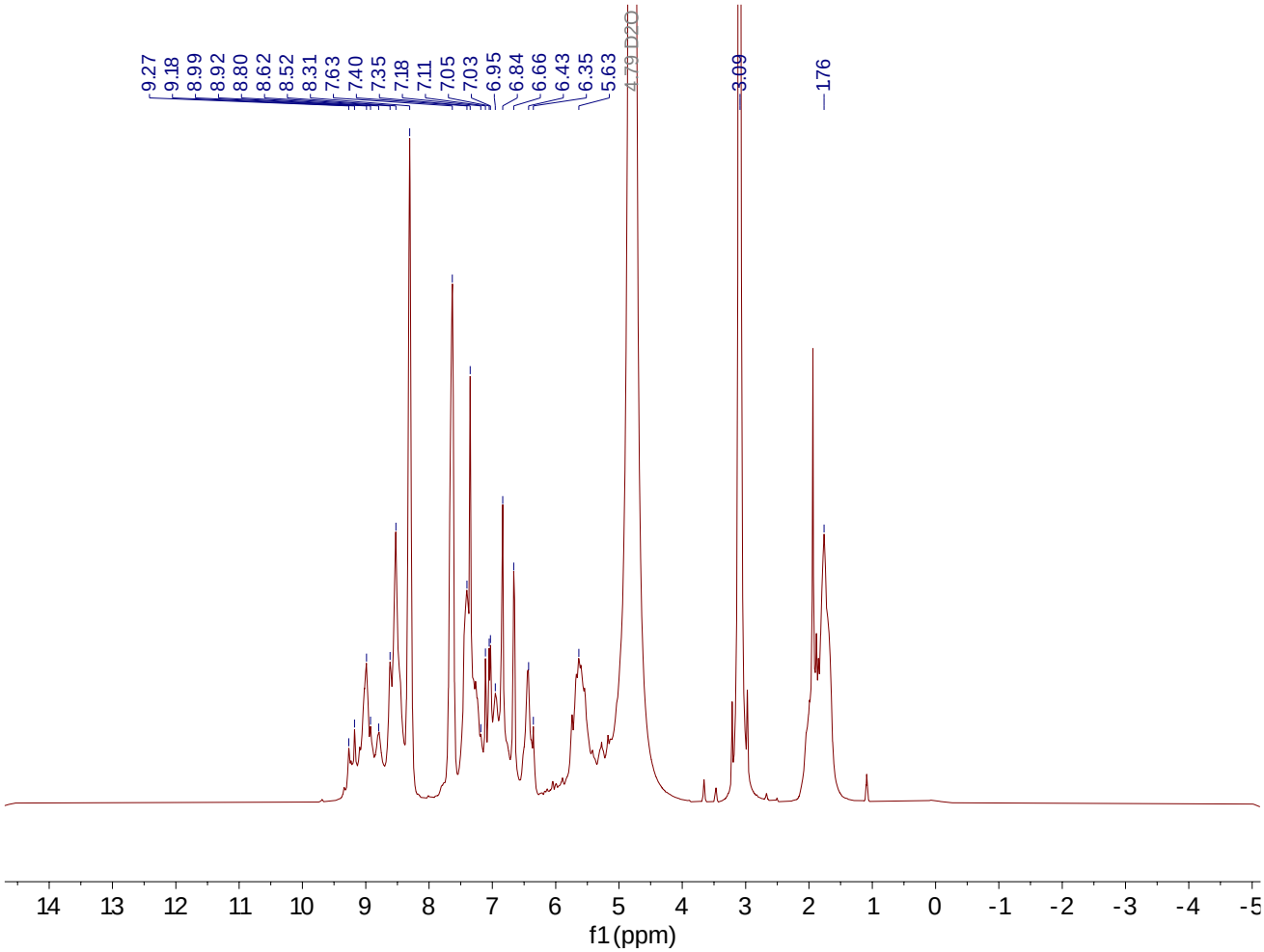

Figure A. 8. 1H-NMR spectrum of the heteroleptic cage library in D2O, measured at 600 MHz. Due to the high degree of peak overlap no integrals were taken.

Complete UV-Vis data for phase transfer

In this section the complete UV-Vis data for the phase transfer of 5 from water to EtOAc using $LiB(C_6F_5)_4$ are presented.

In Table A. 1 and Figure A. 9 the calibration data for cage 4 are presented. The measurements were repeated 3 times and the calibration curve was constructed by doing linear regression on all collected data.

Table A. 1. UV-Vis raw data for cage 5 in water.

Concentration (μM)	Abs at λ=572		
	Series 1	Series 2	Series 3
31.4	1.56	1.56	1.56
25.1	1.25	1.25	1.25
20.1	0.999	0.999	0.999
16.07	0.773	0.773	0.773
12.9	0.620	0.620	0.620
10.3	0.501	0.501	0.501
8.23	0.398	0.398	0.398
6.59	0.312	0.312	0.312
5.27	0.250	0.250	0.250
4.21	0.205	0.205	0.205

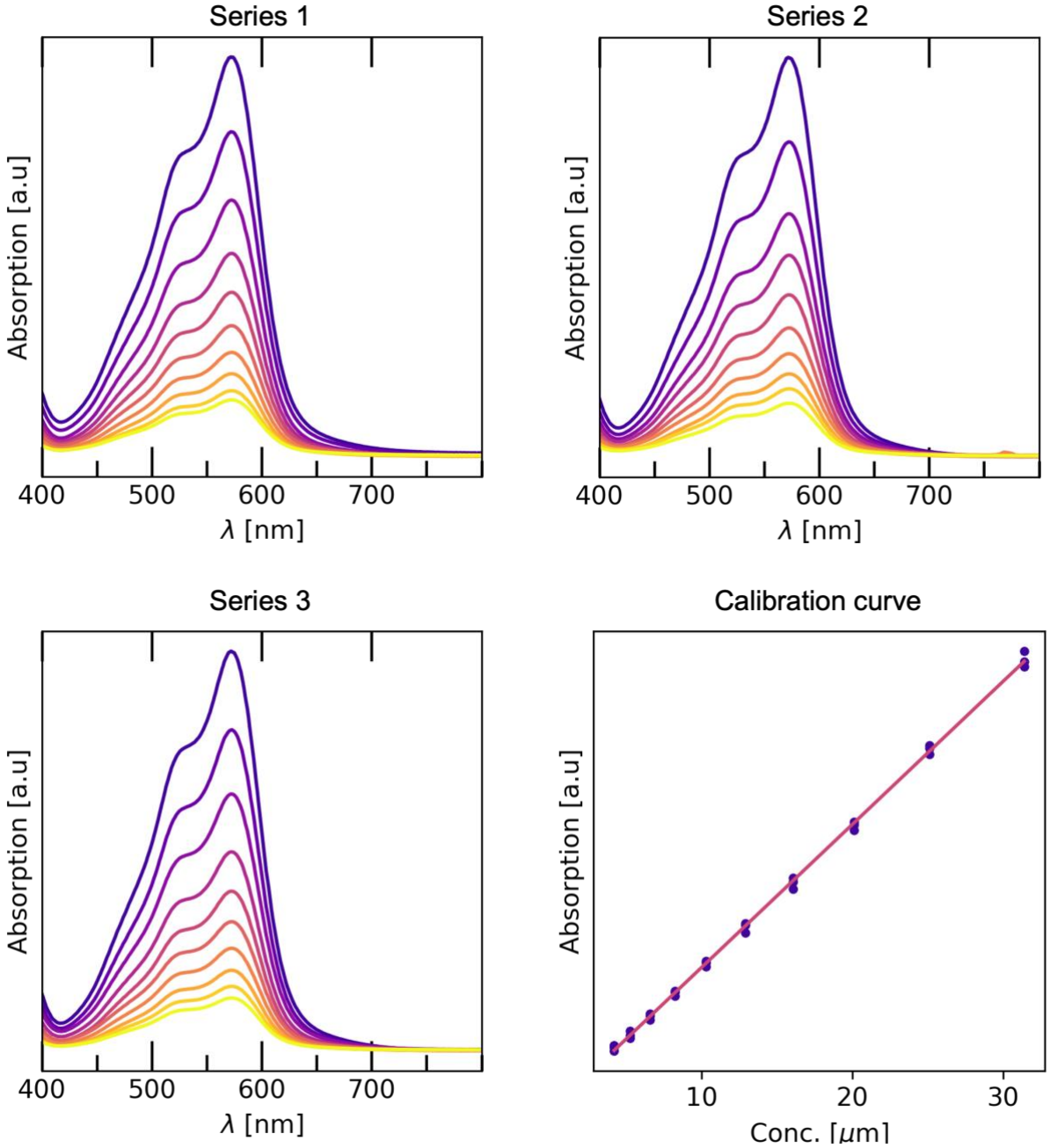

Figure A. 9. Raw UV-Vis data for cage 5 in water, and the calibration curve obtained from these data. Abs=0.05C-0.006

In Figure A. 10 and Table A. 2 the calibration data for cage 5 in EtOAc is shown. The initial solution was made by using a minimum amount of $LiB(C_6F_5)_4$ to transfer all the cage from a 26 µM water solution of the cage, thus the concentration for the first point of the calibration curve was taken to be 26 µM.

Table A. 2. Summary of UV-Vis data for construction of a calibration curve for 4[$B(C_6F_5)_4$] in EtOAc.

Concentration (µM)	Abs at λ=571
26	1.51
20	1.00
16	0.87
13	0.73

10	0.69
8	0.63
6	0.48

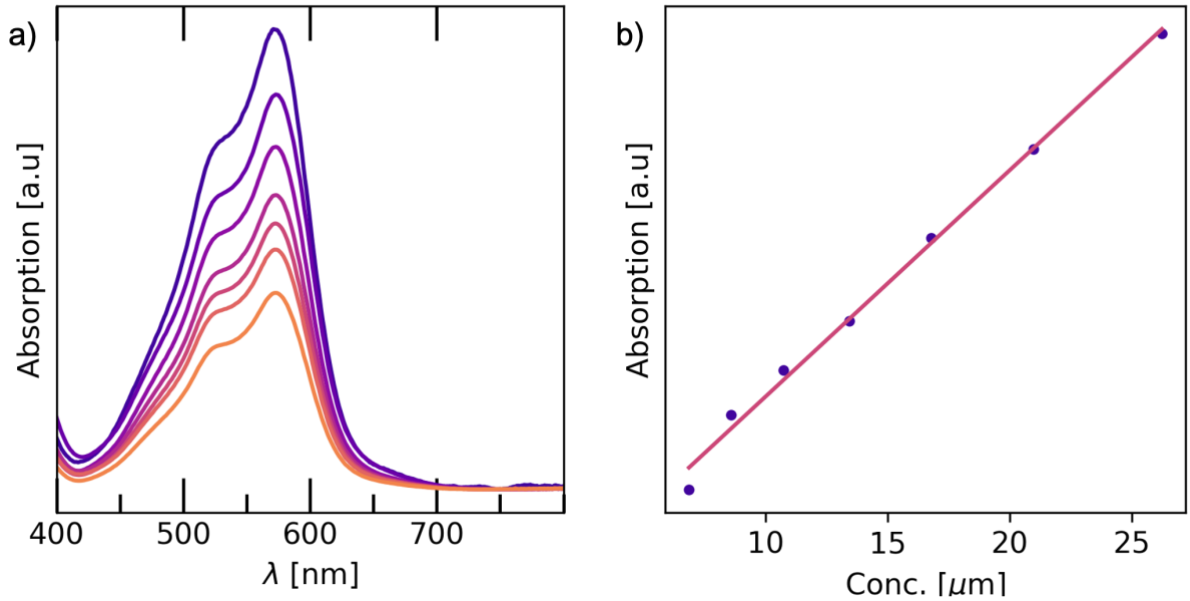

Figure A. 10. a) Raw UV-Vis data for cage 5 in EtOAc. b) Calibration curve for 5 in EtOAc. y=0.01C+0.30

In Table A. 3 and **Error! Reference source not found.**, the UV-Vis raw data for the phase transfer of cage 5 is presented. The correction factors are calculated from the solubility of EtOAc in water.

Table A. 3. Summary of Uv-Vis data for phase transfer of 5 to EtOAc using $LiB(C_6F_5)_4$

Layer	$B(C_6F_5)_4$ eqv.	Abs	$C_{measured}$ (µM)	Correction factor	$C_{corrected}$ (µM) *	Cage proportion (%)
Water (λ_{max}=572)	0	1.493	29.8	1.0625	31.6	100
	1	1.411	28.1	1.0625	29.9	94
	2	1.396	27.8	1.0625	29.6	93
	3	1.250	24.9	1.0625	26.5	83
	4	1.136	22.7	1.0625	24.1	76
	5	0.969	19.4	1.0625	20.6	65
	6	0.812	16.2	1.0625	17.3	54
	7	0.638	12.8	1.0625	13.6	43
	8	0.575	11.5	1.0625	12.3	39
	9	0.450	9.1	1.0625	9.6	30
	10	0.290	5.9	1.0625	6.2	20
	11	0.146	3.02	1.0625	3.2	10
	12	0.0425	1.0	1.0625	1.0	3
	13	0.012	0.35	1.0625	0.38	1
	14	0.040	0.91	0	0	0**
EtOAc (λ_{max}=572)	0	0.0008	-8.9	0	-8.4	0***
	1	0.057	-7.3	0	-6.9	0***
	2	0.090	-6.3	0	-5.9	0***

	3	0.340	1.0	0.9375	0.95	2.6
	4	0.441	4.0	0.9375	3.7	10.1
	5	0.654	10.3	0.9375	9.6	26
	6	0.830	15.5	0.9375	14.5	39
	7	1.01	20.9	0.9375	19.6	53
	8	1.088	23.1	0.9375	21.6	58
	9	1.254	28.0	0.9375	21.6	71
	10	1.575	37.5	0.9375	26.2	95
	11	1.581	37.6	0.9375	35.1	100***
	12	1.647	39.6	0.9375	37.1	100***
	13	1.393	32.06	0.9375	30.1	100***
	14	1.21	26.68	0.9375	25.01	100***

*$C_{corrected}=C_{measured}\cdot$(Correction factor)

**Set to 0, high absorption due to formation of emulsion.

*** Concentation higher than the initial water concentration set to 100%. Negative concentrations set to 0.

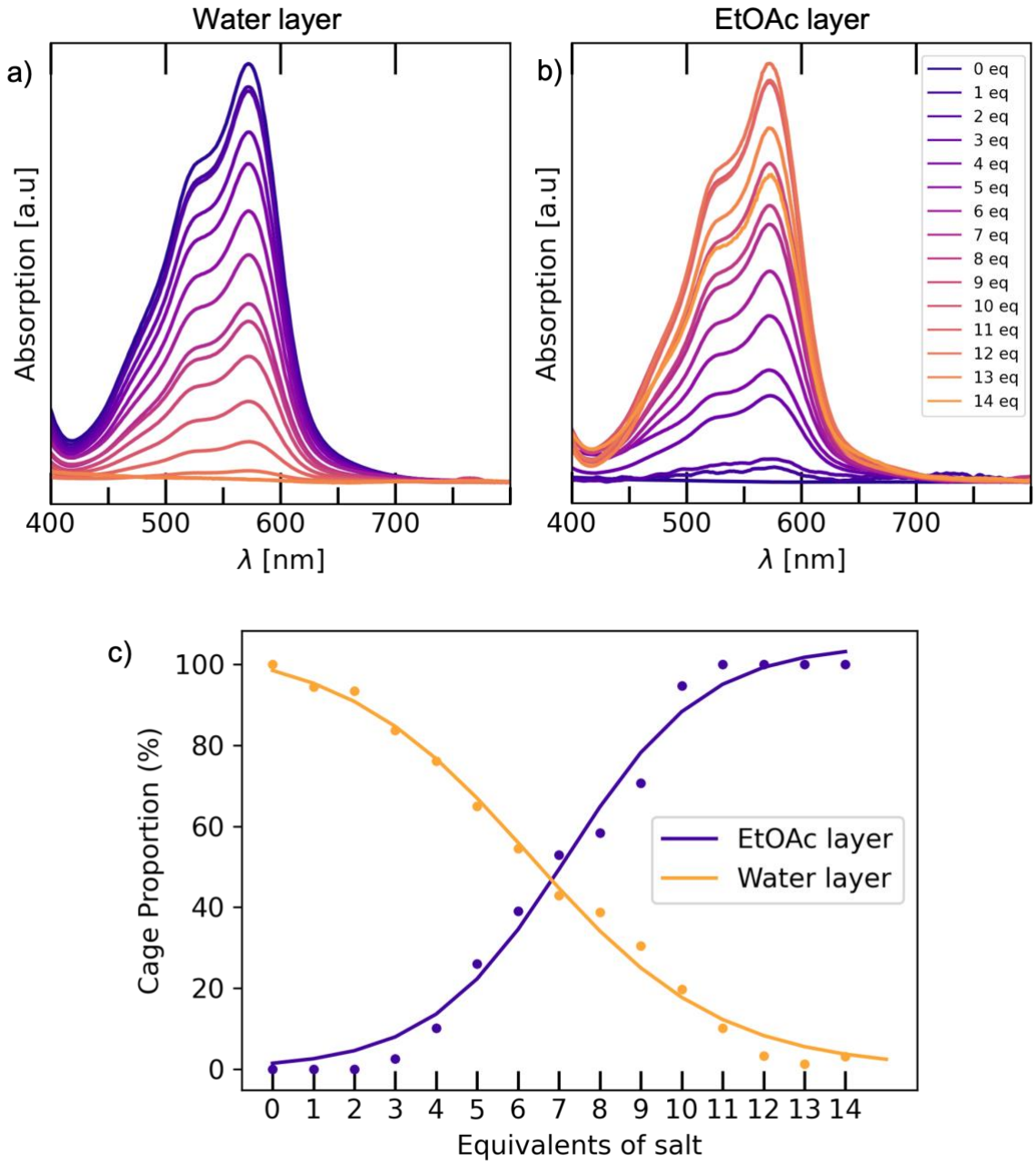

Figure A. 11. Phase transfer data for cage ***5****.a) Raw UV-Vis data for cage* ***5*** *in water. b) Raw UV-Vis data for cage 5 in EtOAc. c) Transfer plot for cage 5, with fitted logistic functions.*

Complete X-ray crystallography data

Crystal Data for cage **5** (M =3537.87 g/mol): monoclinic, space group P21/c (no. 14), a = 28.6608(17) Å, b = 20.599(2) Å, c = 31.1794(15) Å, β = 102.516(6)°, V = 17971(2) Å3, Z = 4, T = 116(9) K, μ(Cu Kα) = 4.022 mm-1, Dcalc = 1.308 g/cm3, 71324 reflections measured (5.18° ≤ 2Θ ≤ 122.798°), 26266 unique (Rint = 0.3147, Rsigma = 0.3383) which were used in all calculations. The final R1 was 0.2835 (I > 2σ(I)) and wR2 was 0.6435 (all data).

Empirical formula	$C_{156}H_{124}F_{30}Fe_4N_{24}P_5$
Formula weight	3537.87
Temperature/K	116(9)
Crystal system	monoclinic
Space group	$P2_1/c$
a/Å	28.6608(17)
b/Å	20.599(2)
c/Å	31.1794(15)
α/°	90
β/°	102.516(6)
γ/°	90
Volume/Å^3	17971(2)
Z	4
ρ_{calc}g/cm^3	1.308
μ/mm^{-1}	4.022
F(000)	7176.0
Radiation	Cu Kα (λ = 1.54184)
2Θ range for data collection/°	5.18 to 122.798
Index ranges	-32 ≤ h ≤ 29, -22 ≤ k ≤ 22, -35 ≤ l ≤ 32
Reflections collected	71324
Independent reflections	26266 [R_{int} = 0.3147, R_{sigma} = 0.3383]
Data/restraints/parameters	26266/0/909
Goodness-of-fit on F^2	1.466
Final R indexes [I>=2σ (I)]	R_1 = 0.2835, wR_2 = 0.5684
Final R indexes [all data]	R_1 = 0.4724, wR_2 = 0.6435
Largest diff. peak/hole / e Å^{-3}	2.23/-1.20

DEPARTMENT OF CHEMISTRY AND CHEMICAL ENGINEERING
CHALMERS UNIVERSITY OF TECHNOLOGY
Gothenburg, Sweden 20xx
www.chalmers.se

CHALMERS
UNIVERSITY OF TECHNOLOGY